Research article

PG
Petroleum Geoscience

https://doi.org/10.1144/petgeo2022-043 | Vol. 29 | 2023 | petgeo2022-043

The importance of facies, grain size and clay content in controlling fluvial reservoir quality – an example from the Triassic Skagerrak Formation, Central North Sea, UK

Oluwafemi E. Aro[1*], Stuart J. Jones[1], Neil S. Meadows[2], Jon Gluyas[1] and Dimitrios Charlaftis[3]

[1] Department of Earth Sciences, Durham University, Lower Mountjoy, South Road, Durham DH1 3LE, UK
[2] Redrock Associates International, 38 Queens Drive, Prenton, Merseyside CH43 0RP, UK
[3] School of Geosciences, University of Aberdeen, Meston Building, King's College, Aberdeen AB24 3UE, UK
OEA, 0000-0003-0646-0553
* Correspondence: oluwafemi.e.aro@durham.ac.uk

Abstract: Clay-coated grains play an important role in preserving reservoir quality in high-pressure, high-temperature (HPHT) sandstone reservoirs. Previous studies have shown that the completeness of coverage of clay coats effectively inhibits quartz cementation. However, the main factors controlling the extent of coverage remain controversial. This research sheds light on the influence of different depositional processes and hydrodynamics on clay-coat coverage and reservoir quality evolution. Detailed petrographic analysis of core samples from the Triassic fluvial Skagerrak Formation, Central North Sea, identified that channel facies offer the best reservoir quality; however, this varies as a function of depositional energy, grain size and clay content. Due to their coarser grain size and lower clay content, high-energy channel sandstones have higher permeabilities (100–1150 mD) than low-energy channel sandstones (<100 mD). Porosity is preserved due to grain-coating clays, with clay-coat coverage correlating with grain size, clay-coat volume and quartz cement. Higher coverage (70–98%) occurs in finer-grained, low-energy channel sandstones. In contrast, lower coverage (<50%) occurs in coarser-grained, high-energy channel sandstones. Quartz cement modelling showed a clear correlation between available quartz surface area and quartz cement volume. Although high-energy channel sandstones have better reservoir quality, they present moderate quartz overgrowths due to lesser coat coverage, and are thus prone to allowing further quartz cementation and porosity loss in ultra-deep HPHT settings. Conversely, low-energy channel sandstones containing moderate amounts of clay occurring as clay coats are more likely to preserve porosity in ultra-deep HPHT settings and form viable reservoirs for exploration.

Supplementary material: of data and technique used in this study are available at https://doi.org/10.6084/m9.figshare.c.6438450

Received 5 June 2022; **revised** 7 November 2022; **accepted** 20 February 2023

The Triassic Skagerrak Formation sandstones are important hydrocarbon-producing reservoirs in the high-pressure, high-temperature (HPHT) section of the UK North Sea Central Graben, with present-day pore pressure and temperature exceeding 80 MPa and 150°C, respectively (Stricker and Jones 2016; Stricker *et al.* 2016*b*). They exhibit varying degrees of heterogeneity, and contain anomalously high porosity (up to 35%) and permeability (up to 3000 mD), despite their present-day burial depth of 3105–5019 m (10 187–16 467 ft) below sea floor and temperature of over 150°C (Smith *et al.* 1993; Nguyen *et al.* 2013; Akpokodje *et al.* 2017). Previous studies have attributed the anomalously high porosity and permeability in the Skagerrak sandstones to the early onset and continuous increase of overpressure, which limited mechanical compaction, and the presence of chlorite coats, which inhibited quartz cementation during burial diagenesis (Nguyen *et al.* 2013; Stricker and Jones 2016; Stricker *et al.* 2016*b*). However, only a few studies have been published on the distribution of clay coatings as a function of depositional facies (i.e. grain size, sorting and clay content) in these deeply buried sandstones. The HPHT hydrocarbon reservoirs of the UKCS Triassic successions are becoming increasingly attractive for further exploration (McKie and Audretsch 2005; Burgess *et al.* 2020). They are also potential targets for geothermal energy and carbon capture and storage (CCS). Thus, understanding the controls on reservoir quality and, most importantly, clay coat effectiveness is crucial for finding good-quality reservoirs.

The reservoir quality (i.e. porosity and permeability) of deeply buried sandstones is mainly dictated by the combined effect of depositional facies, burial compaction and diagenetic processes (Ajdukiewicz and Lander 2010). Depositional factors (such as grain size, sorting, clay content and detrital composition) exert significant control on sandstone initial depositional porosity and permeability, and influence the extent and distribution of subsequent diagenesis (Baker 1991; Smith *et al.* 1993; Morad *et al.* 2000, 2010; Ajdukiewicz and Lander 2010). Diagenetic processes that control reservoir quality include compaction, cementation (mainly by quartz, clay minerals and carbonates), and dissolution of framework grains and cements. In general, with increasing burial depth, sandstones progressively lose porosity via mechanical compaction. At greater depth, chemical compaction (pressure dissolution) becomes active, resulting in further porosity reduction (Bjørlykke 2014). Quartz is volumetrically the most important pore-occluding diagenetic cement in deeply buried clean sandstone reservoirs (McBride 1989; Ehrenberg 1990; Walderhaug 1996; Worden and Morad 2000; Molenaar *et al.* 2007; Gier *et al.* 2008; Worden *et al.* 2018*a*, *b*). Quartz cementation starts at around 70–80°C (McBride 1989; Bjørlykke and Egeberg 1993; Walderhaug 1994*a*; Storvoll *et al.* 2002; Lander *et al.* 2008; Ajdukiewicz and Lander 2010; Taylor *et al.* 2010; Oye *et al.* 2018). The presence of early formed clay coats (e.g. chlorite) can inhibit quartz cementation by blocking nucleation sites and making the surface area unavailable for pore-occluding quartz overgrowths, thereby preserving anomalously high porosity in deeply buried sandstones (Worden and Morad 2000; Bloch *et al.* 2002; Ajdukiewicz and Larese 2012; Nguyen *et al.* 2013; Stricker and Jones 2016; Worden *et al.* 2020; Xia *et al.* 2020).

The ability of clay coats to effectively inhibit quartz cementation is primarily a function of its completeness or coverage (i.e. fraction of surface area of grains covered by clay minerals) and not just its presence (Ehrenberg 1993; Walderhaug 1996; Bloch *et al.* 2002; Billault *et al.* 2003; Lander *et al.* 2008; Ajdukiewicz and Larese 2012; Stricker and Jones 2016; Charlaftis *et al.* 2021). Detrital clay coats are often interpreted as precursors for authigenic clay coats in deeply buried sandstone reservoirs (Bahlis and De Ros 2013; Verhagen *et al.* 2020). In fluvial settings, the most common ways by which detrital clay minerals (e.g. smectite) are incorporated into fluvial sandstones either as clay coatings or pore-filling clays are by mechanical infiltration of clay-rich waters and inherited grain-coating clays (Matlack *et al.* 1989; Worden and Morad 2003; Dowey *et al.* 2012). With increasing burial, detrital clays are recrystallized to authigenic clays that could either have a positive or negative impact on deep reservoir quality (Morad *et al.* 2010; Mahmic *et al.* 2018; Virolle *et al.* 2019). In general, the distribution of detrital clay minerals, which are precursors for authigenic clay minerals, has been reported to be controlled by depositional processes, at least in shallow-marine (estuarine) depositional environments (Dowey *et al.* 2012, 2017; Wooldridge *et al.* 2017). Therefore, understanding how the completeness of clay coats changes as a function of depositional processes (e.g. grain size, sorting and clay content) is crucial for the prediction of quality reservoirs in deeply buried sandstones.

In this study, we investigate the impact of depositional facies, grain size, clay content and clay coverage on sandstone reservoir quality in two deeply buried sandstone members (Joanne and Judy) of the Triassic Skagerrak Formation, UK Continental Shelf (UKCS) Central Graben. In addition, we model quartz cement using burial–thermal history to understand quartz cement evolution through time and its relationship with clay-coat coverage, and then compare it with measured quartz cement in the studied sandstones. The sandstone members examined in this study are from wells 30/7a-7 (Judy Field) and 30/2c-4 (Jade Field) in Quadrant 30. They form the main producing intervals in the UKCS Skagerrak Formation; however, they exhibit different reservoir qualities. This study also aims to ascertain whether grain size and clay content are viable tools for predicting clay-coat-enhanced reservoir quality in deeply buried and diagenetically complex sandstone reservoirs.

Geological setting

The Central Graben is the southern arm of a NW–SE-trending trilete rift system in the North Sea, with the Viking Graben (VG) as the northern arm and the Moray Firth Basin (MFB) as the western arm (Fig. 1a). At least two major rifting phases led to the development of the Central Graben, one during the Permian–Triassic (290–210 Ma) and the other during the Upper Jurassic (155–140 Ma), the latter being the main rifting episode. The Central Graben is divided into the West and East Central Graben by two main horst blocks, the Forties–Montrose High and the Josephine Ridge (Fig. 1b), and is flanked by the Norwegian basement in the east and UKCS in the west (Gowers and Sæbøe 1985; Glennie 1998; di Primio and Neumann 2008). The main graben system and the medial horst blocks are presently deeply buried due to subsequent post-rift thermal subsidence and sediment inundation that began at the end of the Jurassic rift episode. Today, they are overlain by a 3–4 km-thick sequence of Cretaceous and Cenozoic strata (Grant *et al.* 2014).

The Triassic sediments of the Central North Sea were deposited in a variety of dryland terminal fluvial settings, ranging from relatively

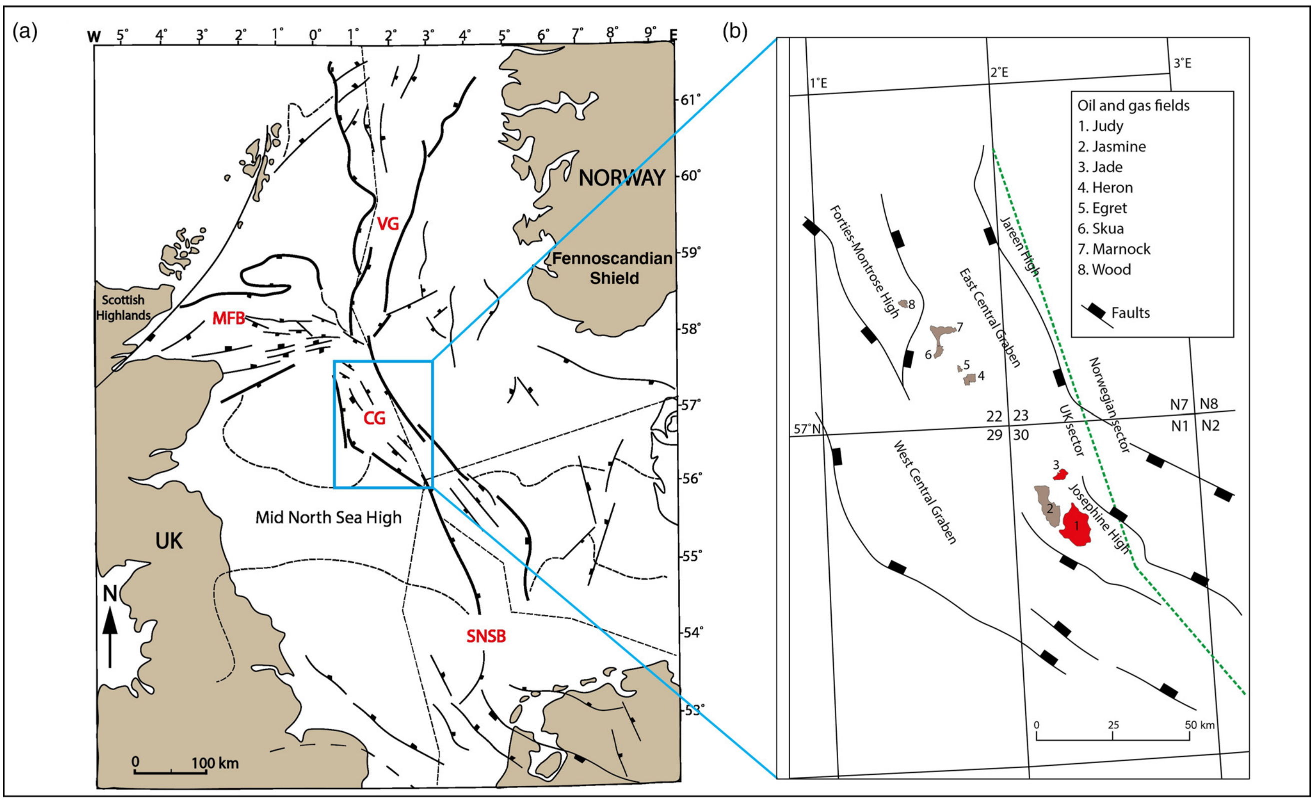

Fig. 1. Location map showing (**a**) the North Sea rift system and its structural elements, with the Moray Firth Basin (MFB), Viking Graben (VG), Central Graben (CG) and Southern North Sea Basin (SNSB) (modified after Brown 1991) and (**b**) the study area (blue box on the structural map), with the Forties–Montrose High (to the NW) and Josephine Ridge horst blocks (to the SE) dividing the Central Graben into the East Central Graben and the West Central Graben. The wells selected for this study are from the fields highlighted in red (Jade and Judy fields).

arid terminal splay and playa to more vegetated, confined-channel systems with associated floodplain facies (McKie *et al.* 2010). Palaeocurrent data reveal that the fluvial drainage pattern was in a north–south direction towards the Southern North Sea, with sediment inputs from the Fennoscandian Shield to the east and the Scottish Highlands to the west (McKie 2011) (Fig. 1a). The deposition of the Triassic sediments occurred directly above an extensive and relatively thick Permian Zechstein salt layer in a series of fault- and salt-controlled minibasins (pods). Early Triassic rifting coupled with sediment loading initiated a widespread syndepositional movement of the underlying Zechstein salt, and this led to the creation of salt-withdrawal minibasins or pods, in which the contemporaneous Triassic sediments accumulated (Hodgson *et al.* 1992; Smith *et al.* 1993). The progressive withdrawal of the salt from beneath the pods into the adjacent salt walls resulted in the continued subsidence of the pods, until they grounded on the underlying Lower Permian Rotliegend faulted basement. The overall thickness of the pods and the rate at which they became grounded vary across the basin and were strongly controlled by the salt thickness. In areas where the salt was initially thin (on basin flanks), the sediment pods grounded early and thus prevented further intrapod deposition and preservation of sediments. In the East and West Central Graben, the salt layer was relatively thick, and the sediment pods did not become grounded until the Late Cretaceous. This allowed the accumulation and preservation of thick sedimentary successions within the pods relative to the interpod areas (Smith *et al.* 1993; Nguyen *et al.* 2013).

The stratigraphic division and nomenclature for the Triassic sequences in the Central North Sea was defined based on detailed biostratigraphic and lithostratigraphic correlation of wells within the J-Ridge area in the South Central Graben (Goldsmith *et al.* 1995, 2003). This stratigraphic correlation has been extended to other areas of the Central North Sea (UKCS quadrants 2 and 29; Norwegian Continental Shelf (NCS) quadrants 7, 15 and 16) through the integration of heavy mineral stratigraphy, seismic and well-log correlation, and high-quality biostratigraphic data (McKie and Audretsch 2005; McKie *et al.* 2010; McKie 2014; Mouritzen *et al.* 2017; Burgess *et al.* 2020). The Triassic of the Central North Sea is divided into two distinct lithostratigraphic units (or formations): the Early Triassic Smith Bank Formation and the Middle–Late Triassic Skagerrak Formation (Fig. 2). The Smith Bank Formation (lower unit), consisting of shales, evaporites and thin sandstones, forms the bulk of the pod infill. The overlying Skagerrak Formation (alternating sandstones and mudstones) occupies the upper section of the pods and the interpod areas. The Skagerrak Formation is further subdivided into three sandstone-dominated members (Judy, Joanne and Josephine) and three mudstone-dominated members (Julius, Jonathan and Joshua) (Goldsmith *et al.* 1995, 2003). The mud-dominated members are thick and laterally extensive within Quadrant 30 but thin northwards and are commonly used as the primary correlation markers for the Skagerrak Formation (McKie and Audretsch 2005). Recent studies of the Triassic stratigraphic framework have, however, proposed a new correlation scheme for the Triassic successions based on the results from high-resolution biostratigraphy and heavy mineral stratigraphy (Mouritzen *et al.* 2017; Burgess *et al.* 2020).

The Triassic Skagerrak Formation underwent a prolonged shallow burial phase (*c.* 150 myr) followed by a rapid burial phase from 90 Ma onwards to their present-day maximum burial depth (Fig. 3). The phase of rapid burial was accompanied by a significant increase in pore pressure and temperature (Stricker *et al.* 2016*b*). The study area (J-Block, UK Quadrant 30) is situated in the southern part of the UK Central Graben (Fig. 1). Throughout the Triassic, this area was at the distal end of a continental clastic (fluvial distributive) system, with sediment originating mainly from the Norwegian mainland but with additional source areas in the Scottish Highlands and Fladen Ground Spur (Steel and Ryseth 1990; Goldsmith *et al.* 1995; Gray *et al.* 2020). The focus of this study is on the Judy and Joanne sandstone members of the Skagerrak Formation in wells 30/07a-7 (Judy Field) and 30/2c-4 (Jade Field). These sandstone members form the main hydrocarbon reservoirs in the Skagerrak Formation and occur in an HPHT environment. In the upper part of the Skagerrak Formation, especially at depths of 4000–5000 m (13 123–16 404 ft) below seafloor (bsf), pore pressures and temperatures exceed 11 603 psi (80 MPa) and 166°C, respectively (Swarbrick *et al.* 2000; di Primio and Neumann 2008; Nguyen *et al.* 2013). Present-day overpressures in the Judy and Jade fields are 3250 psi (22.4 MPa) and 3950 psi (27.2 MPa), respectively (Grant *et al.* 2014) (Table 1).

Methodology

The core samples investigated in this study were chosen from the Judy and Joanne sandstone members of the Triassic Skagerrak Formation in wells 30/7a-7 (Judy Field) and 30/2c-4 (Jade Field), respectively. These two wells were chosen because they contain a variety of fluvial facies with different reservoir properties. A total of 116 core samples (in the form of chips) covering the main depositional facies (Table 2) were chosen from well 30/7a-7 (56 samples) at depths of between 11 291 and 11 548 ft, (measured depth: 3441 and 3519 m) and well 30/2c-4 (60 samples) at depths between 15 585 and 15 793 ft (measured depth: 4750 and 4813 m). The samples were selected at depths that had previously measured porosity and permeability data.

All core samples were vacuum-impregnated with blue-dyed epoxy resin to enhance porosity identification and then made into thin sections. The thin sections were partly stained with Alizarin Red-S and potassium ferricyanide to facilitate the determination of carbonate cement types. Detailed petrographic analysis was conducted on all prepared thin sections, using a Leica DM2500P microscope coupled to a Leica DFC420C digital camera. Thin sections were point counted to determine the percentage of detrital grains, clay matrix, pore-filling and grain-coating cements, and porosity using an automated point-counting stepping stage (PETROG System, Conwy Valley Systems Ltd, Conwy, UK) attached to a Leica petrographic microscope. Modal point-count analysis of the mineral components and porosity was based on 300 point counts per section. Grain size was determined by measuring the long axis of 200 grains (quartz and feldspar) per thin section using the PETROG petrographic software package. Sorting was determined from grain-size measurements using the formula proposed by Folk and Ward (1957). To understand how grain size relates to permeability, the Kozeny equation for estimating permeability from grain size and total porosity (Kozeny 1927; Walderhaug *et al.* 2012) was employed. Measured porosity and permeability data from core analysis were provided by UK Common Data Access (CDA). Core-plug porosity measurements were made using a Boyle's law helium porosimeter. Air permeability measurements were performed using nitrogen gas as a flowing fluid at a confining Hassler pressure of 250 psi. The term 'thin-section porosity' (also known as macroporosity or visible porosity) used in this study is derived from point counting, and refers to the sum of intergranular porosity and intragranular porosity. Helium porosity (i.e. measured/core-plug porosity), on the other hand, is the sum of macroporosity and microporosity. In this study, microporosity is estimated by subtracting the thin-section porosity from the helium porosity. Data from point-count analysis was used to calculate the intergranular volume (IGV). This is defined as the sum of intergranular porosity, depositional matrix and intergranular cement in sandstone samples, and is used to measure compaction in sandstones. Porosity loss due to compaction (COPL) and porosity loss due to cementation (CEPL) were calculated following the

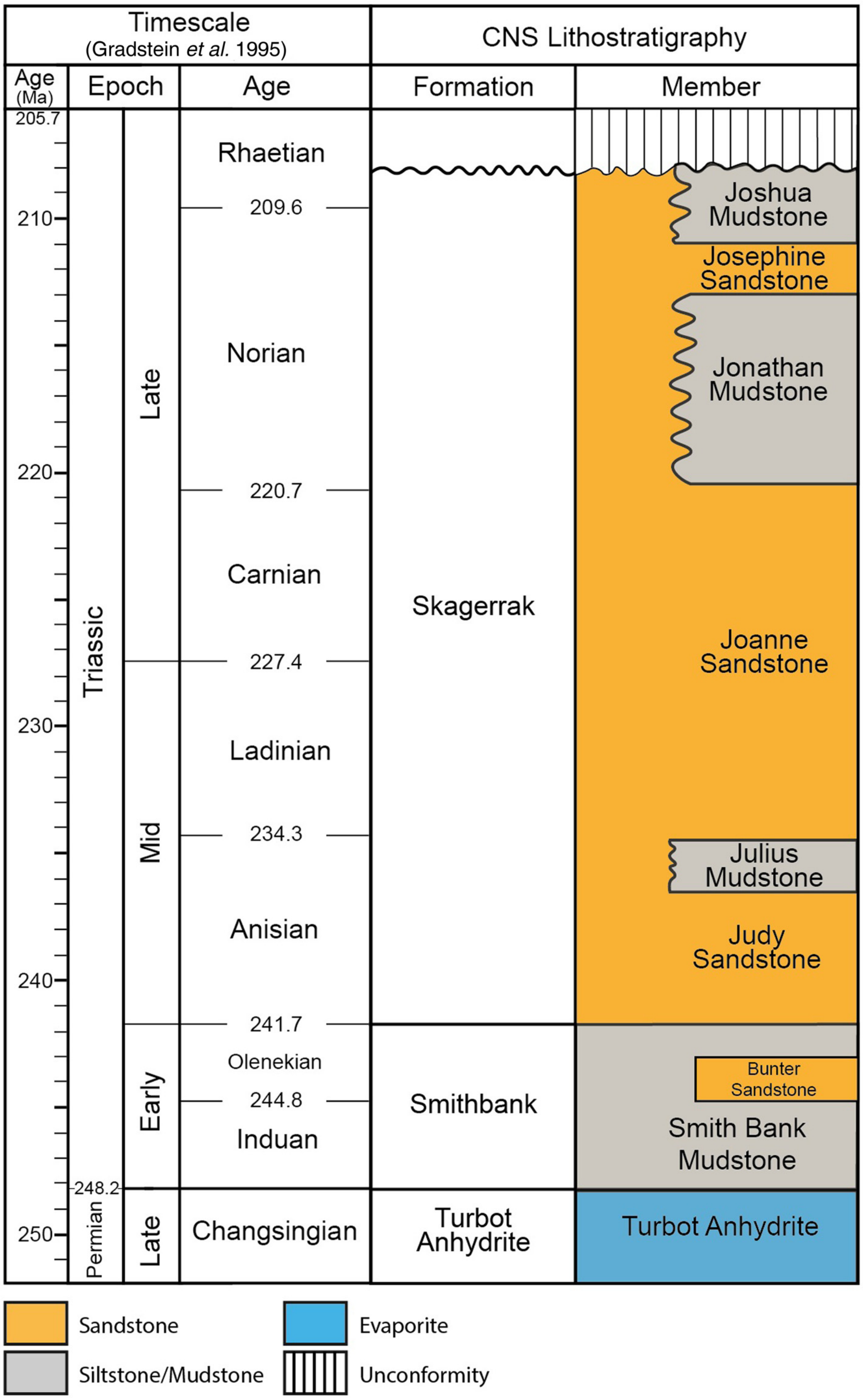

Fig. 2. Central North Sea (CNS) Triassic stratigraphic column showing the six lithostratigraphic members of the Skagerrak Formation (after Goldsmith *et al.* 2003) and their respective ages (after Gradstein *et al.* 1995).

methodology described in Lundegard (1992):

$$\mathrm{COPL} = P_{\mathrm{initial}} - \{[(100 - P_{\mathrm{initial}})\mathrm{IGV}]/(100 - \mathrm{IGV})\}$$
$$\mathrm{CEPL} = (P_{\mathrm{initial}} - \mathrm{COPL})(C/\mathrm{IGV})$$

where P_{initial} is the initial depositional porosity, assumed to be 45%; IGV is the intergranular volume; and C is the intergranular cement.

The detailed point-count results, petrographic information (including IGV, COPL and CEPL), and laboratory measured porosity and permeability are presented in the Supplementary material: Tables S1 and S2.

To investigate the occurrence and morphology of clay minerals in the studied sandstones, 23 sandstone samples with a clay volume between 1 and 11% (based on point counting) were selected from both wells for scanning electron microscopy (SEM) analysis. The selected samples were polished to 30 µm, carbon-coated and examined under a Hitachi SU-70 scanning electron microscope equipped with backscatter (BSE) and an energy-dispersive X-ray (EDX) spectrometer at an accelerating voltage of 10–15 kV and working distance of 15 mm. The EDX system was used to identify the chemical compositions and the distribution of the clays and other minerals in the samples. Furthermore, using montaged SEM/BSE images and high-resolution photomicrographs of the 23 selected sandstone samples, two major clay-coat properties affecting reservoir quality (i.e. clay-coat coverage and thickness) were measured on 150 quartz grains per sample using JMicroVision software (https://jmicrovision.github.io/). The clay-coat coverage (i.e. the fraction of the surface area of grains covered by clay

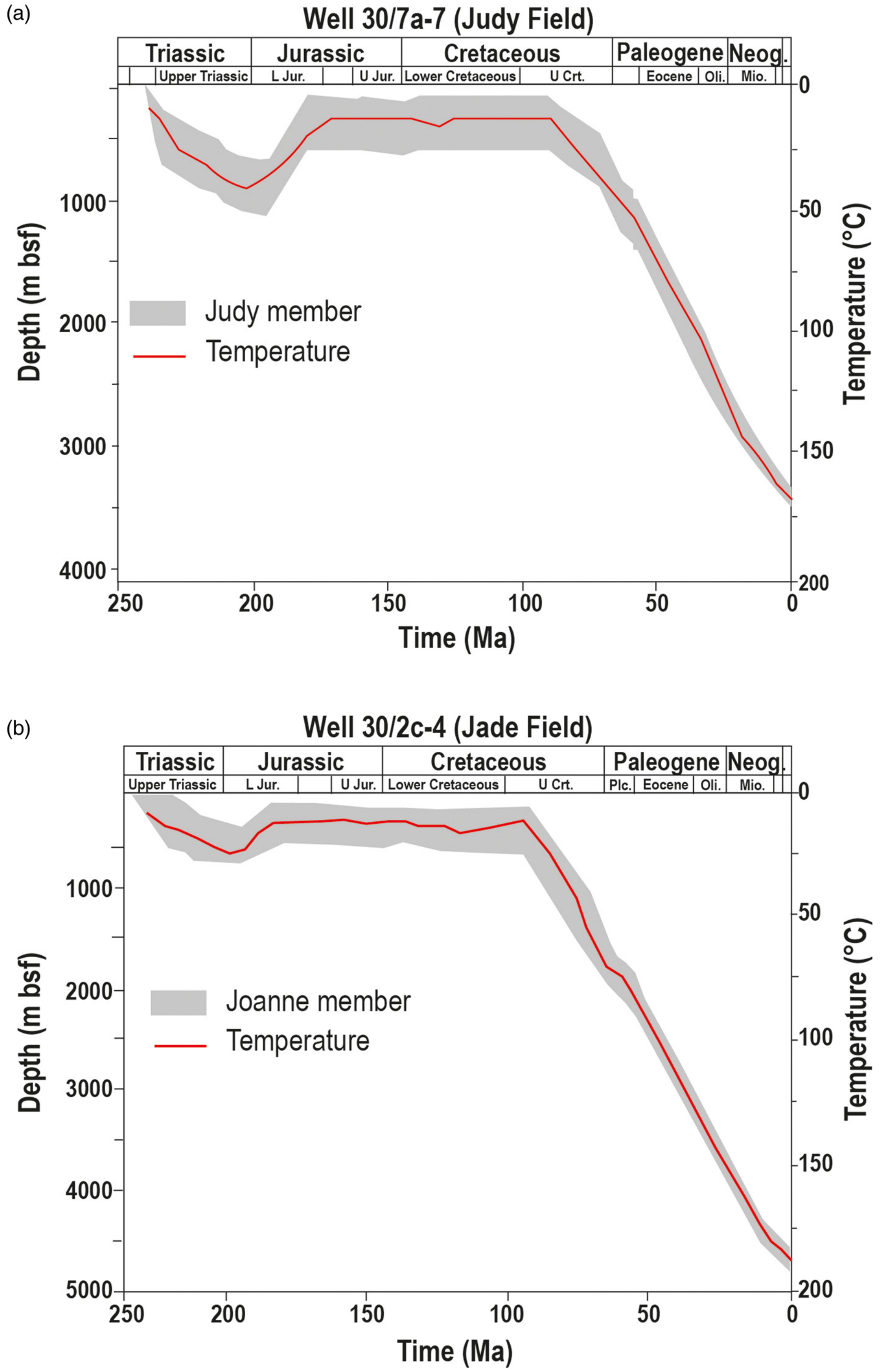

Fig. 3. Burial history and temperature evolution plots for the Judy and Joanne sandstone members in the Judy (well 30/7a-7) and Jade (well 30/2c-4) fields.

minerals) on detrital quartz grains was measured using the perimeter tool in the JMicroVision software, following the procedure proposed by Dutton *et al.* (2018) (see the Supplementary material: Fig. S1). In addition, the clay-coat thickness was measured using the line selection tool in the software. Where clay-coat thickness varies along a grain surface, several thickness measurements were taken and an average thickness value was calculated.

The burial–thermal history curves of the two wells (30/7a-7 in the Judy Field and 30/2c-4 in the Jade Field) were constructed using Schlumberger's PetroMod® (v. 2012.2) 1D basin-modelling software. The software uses a forward modelling approach to calculate the geological evolution of a basin and burial history of a reservoir, especially the temperature and pore fluid pressure evolution of the reservoir. Although the technique is limited in its ability to model overpressure generation from the effect of lateral fluid flow, diagenetic processes and hydrocarbon charging, it can effectively simulate overpressure generation from disequilibrium compaction and pore fluid expansion. Present-day stratigraphy, well-log lithology and lithological descriptions were used to set the 1D burial models (Knox and Holloway 1992; Cameron 1993; Johnson and Lott 1993; Richards *et al.* 1993; Goldsmith *et al.* 1995, 2003). Palaeobasement heat flow was assumed according to Allen and Allen (2005), with a heat flow of 63–110 mW m^{-2} (average 80 mW m^{-2}) during synrift phases and 37–66 mW m^{-2} (average 50 mW m^{-2}) during post-rift phases. The burial history models were calibrated against present-day repeat formation tester (RFT) temperature measurements corrected after Andrews-Speed *et al.* (1984), and measured Skagerrak Formation porosities. They were then carefully adjusted to present-day formation pressure measurements, taking into account late-stage, high-temperature overpressure

Table 1. *Well data from wells 30/7a-7 (Judy Field) and 30/2c-4 (Jade Field) used in this study*

Field			Judy	Jade
Well			30/7a-7	30/2c-4
Depth interval		(ft)	11 291–12 655	15 354–16 675
		(m)	3441–3857	4680–5083
		(TVDSS ft)	11 219–12 572	14 964–16 276
		(TVDSS m)	3420–3832	4561–4961
Water depth		(ft)	249	262
		(m)	76	80
Top reservoir		(TVDSS ft)	11 219	14 964
		(TVDSS m)	3420	4561
Overpressure		(psi)	3250	3950
		(MPa)	22.4	27.2
RFT temperature	Measured	(°C)	143.3	163.8
	Corrected	(°C)	164.1	187.7
	Depth	(TVDSS ft)	12 572	15 566
		(TVDSS m)	3832	4745
No. of core samples			56	60
Sandstone Member			Judy	Joanne

Included are water depth, top reservoir depth, overpressure, and repeat formation tester (RFT) temperatures based on Grant *et al.* (2014). TVDSS, true vertical depth subsea.

mechanisms (i.e. disequilibrium compaction and pore fluid expansion) (Osborne and Swarbrick 1997; Isaksen 2004).

Quartz cementation models for the Judy and Jade field sandstones (Judy and Joanne) were built using the approach of Walderhaug (1996). This mathematical kinetic model calculates the rate of quartz cementation using a logarithmic function, and assumes that compaction terminates at the onset of quartz cementation and the stabilization of framework grains (Walderhaug 1996, 2000). The model incorporates grain size, percentage of grain coatings (i.e. coverage), detrital mineralogy (i.e. detrital quartz fraction) and available quartz surface area, all of which were quantified using the acquired petrographic data. The model also incorporates temperature and burial history, both of which were modelled using PetroMod® (v. 2012.2). Time–temperature histories generated were used to calculate the heating rates incorporated into the cementation models. In order to incorporate grain-coat data into the model, the initial quartz surface area was reduced using the clay-coat coverage data from the samples. The kinetic model was generated using Walderhaug's (1996) standard parameters on 1 cm^3 of sandstone, with an 80°C threshold temperature for quartz cementation and a starting porosity of 26% at the onset of quartz cementation. A value of 1.98×10^{-22} mol cm^{-2} s^{-1} was used for the pre-exponential constant a, and 0.022°C for the exponential constant b, as calculated by Walderhaug (1994*b*) for some North Sea sandstones. Twenty-one samples of similar facies (i.e. channel sandstones) were used in the model: eight samples from the Judy Sandstone Member (well 30/7a07 in the Judy Field) and 13 samples from the Joanne Sandstone Member (well 30/2c-4 in the Jade Field) (see the Supplementary material: Table S3).

Results

Facies description and classification

Eight sedimentary facies were identified in the studied cored intervals from the Judy (well 30/7a-7) and Joanne (well 30/2c-4) sandstone members of the Skagerrak Formation based on grain size, lithology and sedimentary structures (Table 2). These facies types have been classified into three main facies associations comprising: (1) confined fluvial channels (FC); (2) unconfined fluvial splays and sheetfloods (SF); and (3) floodplain, palaeosols and lakes (FL) (Table 3). A schematic fluvial depositional model illustrating the

Table 2. *Classification and description of identified facies in the Judy and Joanne sandstone members from wells 30/7a-7 (Judy Field) and 30/2c-4 (Jade Field)*

Code	Facies	Description
S1	Parallel-laminated/current-rippled sandstones	Very-fine- to fine-grained sandstones with planar parallel lamination and well-defined current ripples with thin silty drapes defining laminae. Rippled bedsets define a low-angle cross-stratification parallel to sparse planar lamination
S2	Massive sandstone	Moderately to well-sorted, fine- to medium-grained massive sandstones with thickness ranging from 0.3 to 2.5 m
S3	Cross-laminated/bedded sandstones	Very-fine- to medium-grained, moderately to well-sorted sandstones forming stacked decimetre- to metre-scale cross-stratified sets with planar erosive set boundaries
S4	Mottled, bioturbated and pedoturbated sandstones	Very-fine- to fine-grained mottled sandstones with evidence of bioturbation resulting in disrupted bedding. Composed of localized dolocrete nodules and dolomite cements
C	Intraformational conglomerate and gravelly sandstone	Poorly sorted sandstones containing pebble-sized clasts with size ranging from 2 to 8 mm. The pebbles are primarily composed of dolocrete and mudclasts, and often occur in channel bases
M1	Mottled and bioturbated mudstone	Grey or green/red-coloured bioturbated silty mudstone facies with frequent mottling
M2	Pedoturbated mudstones and siltstones	Silty mudstones with pervasive carbonate nodules. Commonly mottled, greenish in colour, locally reddened, frequently bioturbated and rootletted with occasional preservation of current rippling and planar parallel lamination.
M3	Laminated mudstone	Mid- to dark-grey finely laminated argillaceous siltstone/mudstone with thin laminae and lenses of laminated or current-rippled very-fine sandstone

Table 3. *Facies association scheme used in this study and their colour codes*

Facies association	End members	Facies code	Colour code
Confined fluvial channel (FC)	High-energy fluvial channel (HEFC)	S1, S2, S3, S4, C	
	Low-energy fluvial channel (LEFC)	S1, S2, S3, S4, C	
Unconfined fluvial splays and sheetfloods (SF)		S1, S2, S4, M1, M2, C	
Floodplain, palaeosols and lakes (FL)		S4, M1, M2, M3	

subenvironments and different facies associations identified is shown in Figure 4. Figures 5–7 show the sedimentary logs for the two wells, representative cores and thin-section images of the identified sedimentary facies, respectively.

Confined fluvial channel (FC)

Sandstone sequences representing the fill of fluvial channels are highly variable but range between distinctive end members (i.e. high and low energy) based on grain size and bedform scale, all of which overlie sharp-based erosional surfaces commonly defined by intraformational conglomerates (C). The more abundant of these types comprise moderately to well-sorted, fine- to medium-grained sandstones, forming decimetre- to metre-scale, moderate- to high-angle cross-stratified beds (S3) (Fig. 6). These are often stacked, forming channel-filling sequences of up to more than 23 ft (7 m) in thickness. Channel fills of this type are more common in the Joanne Sandstone and rare in the Judy Sandstone Member. Both the dominant grain size (fine sand) and the scale of the bedforms suggest that most of these channel-filling sandstones were deposited under conditions of high flow competence in active streams and represent bar-scale bedforms. Similar characteristics have been ascribed to deposition within low- to moderate-sinuosity channels (Bridge and Lunt 2006) but, for the purposes of this paper, they are referred to as high-energy fluvial channel (HEFC) sandstones.

At the opposite end of the spectrum of channel fills are sequences that commonly exhibit a marked upward fining. They similarly tend to overlie intraclastic conglomerates (C) resting on sharply erosive channel bases but are dominated by very fine to fine sandstones forming low-angle decimetre-scale beds, planar lamination, and current and wave rippling (S1) (Fig. 6). Where complete, the channel-filling sequences can equally range up to more than 23 ft (7 m) in total thickness but commonly pass upwards into highly argillaceous very fine sandstones and siltstones that are locally disrupted by either or both bioturbation and pedoturbation. The finer grain sizes (i.e. very fine sand) and a range of sedimentary structures indicate significantly lower energy levels and stream competence at the time of deposition. While sandstone sequences of the corresponding type have been interpreted to represent higher sinuosity channels (Leeder 1973; Bridge *et al.* 1995; Wu *et al.* 2015, 2016), in this paper, they are referred to as low-energy fluvial channel (LEFC) sandstones.

The channel-filling sandstone sequences occurring within the Joanne and Judy sandstone members are intermediate in character between the two end members described above. However, the samples used in this study can be assigned with confidence to the two end members. It is therefore proposed that the terms high-energy fluvial channels (HEFC) and low-energy fluvial channels (LEFC) best serve the purposes of the assessments of reservoir quality within the present contribution (Fig. 5a, b).

Unconfined fluvial splays and sheetfloods (SF)

This facies association mainly comprises very-fine- to fine-grained, variably argillaceous and micaceous sandstones, and silty mudstones (Figs 5 and 7e, f). The sandstone components are characterized by planar lamination and current ripples with thin silty/mica drapes (S1). The sandstone units of this facies association commonly occur as weakly defined coarsening-upward sequences or upward-fining packages that are less than 1 ft (0.3 m) and up to 7 ft (2 m) thick. They are usually interbedded with argillaceous silty mudstones of facies M1–M3. The splay facies of the Skagerrak Formation have been interpreted as unconfined sheetflood deposits, which either form as crevasse (adjacent to river channels) or terminal splay (McKie and Audretsch 2005; McKie 2011; Akpokodje *et al.* 2017; Gray *et al.* 2020). The micaceous splay

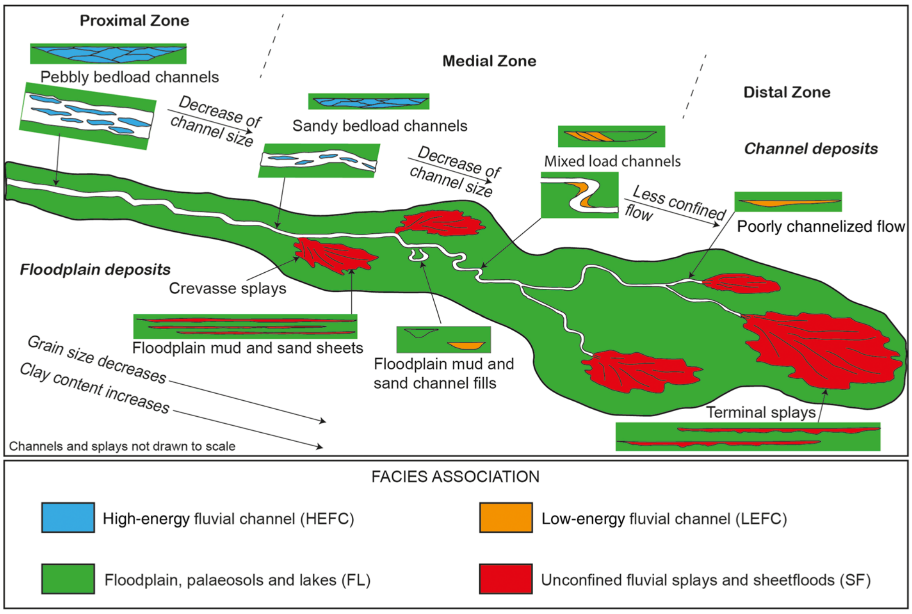

Fig. 4. A schematic fluvial depositional model illustrating the subenvironments and different facies associations identified in this study (modified after Nichols and Fisher 2007).

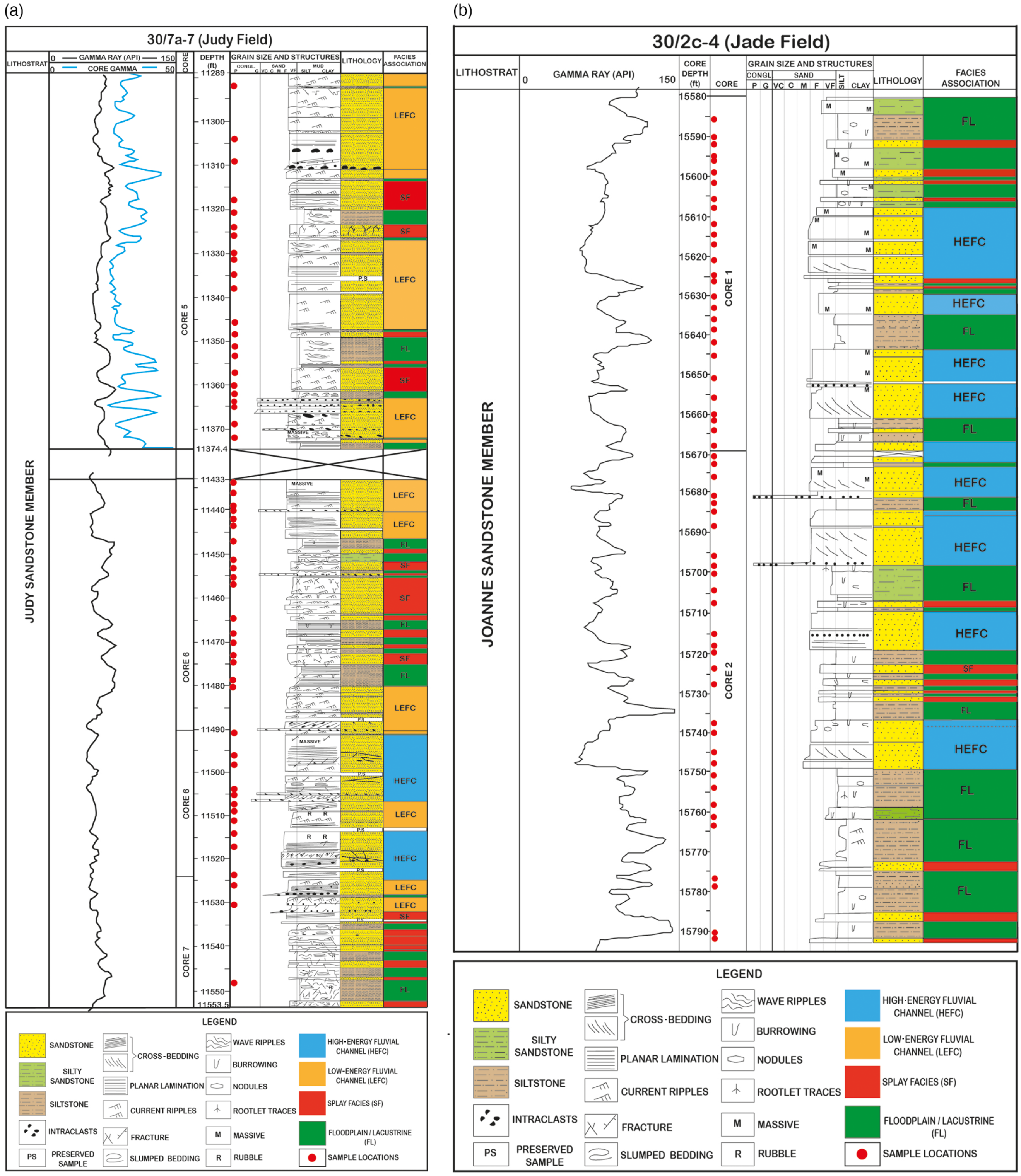

Fig. 5. Sedimentary log of (**a**) well 30/7a-7 (Judy Field) and (**b**) well 30/2c-4 (Jade Field) showing the interpreted facies association based on lithology, grain size and sedimentary structures. Corresponding gamma-ray logs of the cored intervals and core sample locations are also shown.

sandstone facies are interpreted to depict more proximal sheetflood deposits, while the argillaceous and highly micaceous splay sandstones correspond to more distal sedimentation.

Floodplain, palaeosols and lakes (FL)

The sediment packages characterizing this facies association generally include silt- to clay-grain-sized siltstones and mudstones (Figs 5 and 7j–l). They significantly contain pedogenic carbonate nodules (e.g. dolocrete), suggested to be reworked as clasts within channel bases, influencing the distribution of carbonate cements. They are usually mottled, bioturbated and pedoturbated. Common sedimentary structures include current or wave ripples, and parallel laminations, where not overprinted by bioturbation and pedoturbation. The sediments of this facies association are generally associated with fluvial channel and splay facies, and can form thicker units up to 27 ft (8 m). The floodplain facies (M1 and M2: Fig. 6) represent sediments deposited in low-energy environments and/or distal parts of sheetflood and splay facies. The lacustrine facies (M3: Fig. 6) represent depositions within abandoned

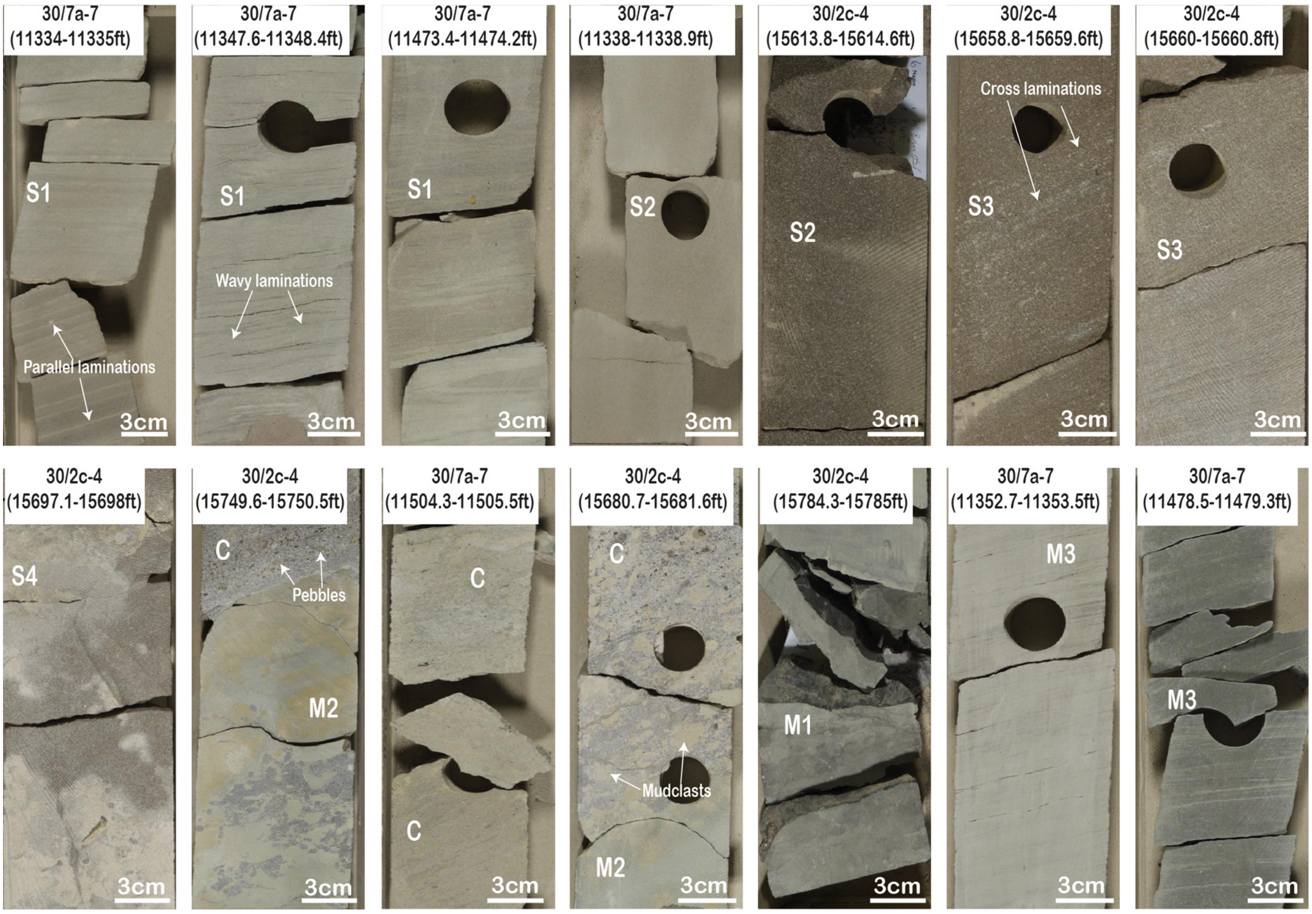

Fig. 6. Representative core photographs of the identified facies. S1, parallel-laminated/current-rippled sandstones; S2, massive sandstones; S3, cross-laminated/bedded sandstones; S4, mottled, bioturbated and pedoturbated sandstones; C, intraformational conglomerates and gravelly sandstones – the dark green pebbles represent reworked dolocrete nodules sourced from adjacent floodplain facies (M2); M1, mottled and bioturbated mudstone; M2, pedoturbated mudstones and siltstones; M3, laminated mudstone.

channels or lakes created by salt tectonic subsidence. The presence of dolocrete nodules in these deposits is indicative of pedogenesis resulting from lowering of the water table and prolonged subaerial exposure in an arid setting (Akpokodje *et al.* 2017; Gray *et al.* 2020).

Detrital texture and composition

The Skagerrak sandstones are very fine–medium grained (Fig. 8) and range from moderately well sorted (0.5–0.71) to very well sorted (<0.35) according to the classification of sorting degree proposed by Folk and Ward (1957). The sandstones are subarkosic to lithic arkosic in composition (Folk 1980) (Fig. 9). Compositionally, the sandstones (i.e. Judy and Joanne) are immature, and have an average composition of 55% quartz, 39% feldspar and 6% rock fragments. Quartz grains comprise both monocrystalline and polycrystalline quartz but are mostly monocrystalline. The feldspar grains include K-feldspar, plagioclase (of an albitic composition) and trace amounts of microcline. Associated rock fragments include igneous and metamorphic rocks. Intrabasinal mudclasts and dolocrete nodules are also common and more abundant at channel bases (Fig. 7j). Detrital micas (muscovite and biotite) range from 0.7 to 19.6% (average 6.2%) and from 0.3 to 8.3% (average 2.7%) in the sandstones of the Judy and Joanne members, respectively. They are, however, more abundant in SF sandstones than in HEFC and LEFC sandstones in both members (Tables 4 and 5). In addition to detrital micas, other accessory minerals recognized during the SEM analysis include rutile, apatite and zircon but these occur in trace amounts within the samples.

Both sandstone members (Judy and Joanne) are compositionally similar. However, they have different average grain sizes and total amount of clay (detrital/authigenic). Sandstones from the Joanne Sandstone Member are, on average, coarser compared to those from the Judy Sandstone Member (Table 6; Fig. 8). Judy Sandstone Member sandstones are made up of LEFC, HEFC and SF sandstone facies, and have an average grain size of 0.102 mm (upper very fine sand). Joanne Sandstone Member sandstones, on the other hand, are composed of HEFC and SF sandstone facies, and have an average grain size of 0.19 mm (upper fine sand) (Tables 4–6). The detrital clay matrix consists of clay minerals mixed with silt-sized quartz and feldspar. The clays consist of chlorite and illite, with moderately high birefringence and greenish to brown colour. In this study, it is sometimes difficult to distinguish detrital clays from authigenic clays due to their diagenetic recrystallization. Thus, for simplicity, the clays have been classified into pore-filling and grain-coating clays. The total clay content varies from 5.6 to 46.9% in the Judy Sandstone Member sandstones and 1.3–36.2% in the Joanne Sandstone Member sandstones, based on point count data (Table 6). Pore-filling clays vary from 0 to 37.6% (average 9.7%) and from 0 to 33.6% (average 8.9%) in the Judy and Joanne member sandstones, respectively. Grain-coating clays vary from 0.3 to 17.4% (average 6.6%) in the Judy Sandstone Member sandstones and from 0.3 to 8.3% (average 3.6%) in the Joanne Sandstone Member sandstones (Table 6). Generally, the HEFC and LEFC sandstones in both members have a lower average clay content than their SF counterparts. In addition, the LEFC sandstones, on average, have a higher total clay content compared to the HEFC sandstones (Tables 4 and 5).

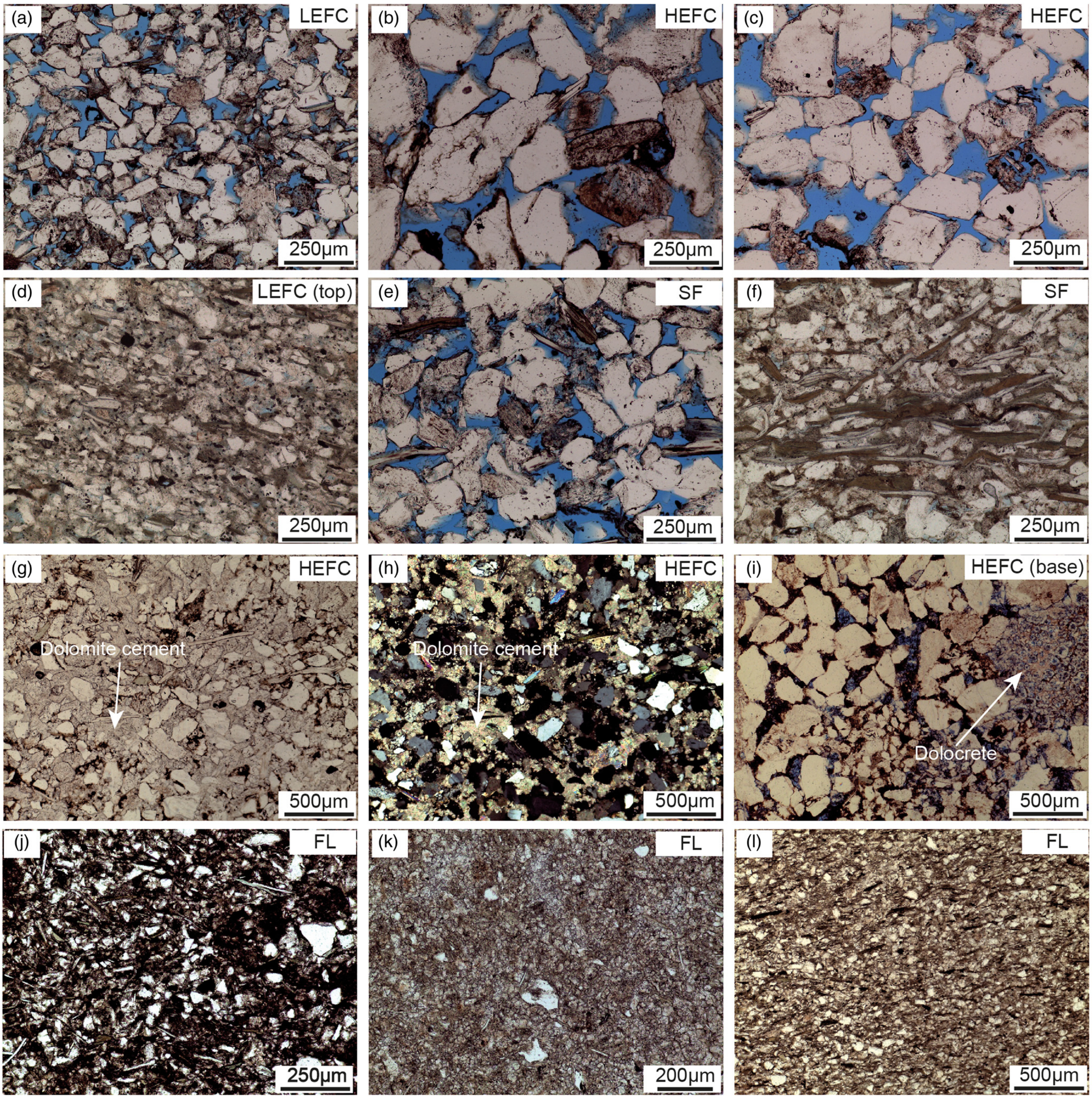

Fig. 7. Representative thin-section photomicrographs of the various facies and their reservoir properties (ϕ, porosity; K_h, permeability; PPL, plane-polarized light; XPL, cross-polarized light; n/a, not applicable). (**a**) Facies S1: very-fine-grained sandstone (30/7a-7); ϕ, 25.7%; K_h, 45 mD; depth, 11 335 ft (3454.9 m). (**b**) Facies S2: medium-grained sandstone (30/2c-4); ϕ, 25.4%; K_h, 890 mD; depth, 15 614.17 ft (4759.2 m). (**c**) Facies S3: upper fine-grained sandstone (30/2c-4); ϕ, 23%, K_h, 1050 mD; depth, 15 660 ft (4773.2 m). (**d**) Facies S1: very-fine-grained current-rippled sandstone (30/7a-7); ϕ, 18.1%; K_h, 3.1 mD; depth, 11 480 ft (3499.1 m). (**e**) Facies S1: lower fine-grained sandstone (30/7a-7); ϕ, 23.5%, K_h, 166 mD; depth, 11 468.3 ft (3495.6 m). (**f**) Facies S1: very-fine-grained current-rippled sandstone (30/7a-7); ϕ, 6.9%; K_h, 0.01 mD; depth, 11 360.1 ft (3462.6 m). (**g**) Facies S4: upper fine-grained pedoturbated sandstone – PPL (30/02c-4); ϕ, 13.3%; K_h, 2.6 mD; depth, 15 697 ft (4784.5 m). (**h**) Facies S4: upper fine-grained pedoturbated sandstone – XPL (30/2c-4); ϕ, 13.3%; K_h, 2.6 mD; depth, 15 697 ft (4784.5 m). (**i**) Facies C: (30/2c-4) ϕ, 4.9%; K_h, 0.04 mD; depth, 15 681 ft (4779 m). (**j**) Facies M1: (30/2c-4); ϕ, 6.3%; K_h, 0.014 mD; depth, 15 778 ft (4809 m). (**k**) Facies M2: (30/2c-4); ϕ, 6.7%; K_h, 0.017 mD; depth, 15 682 ft (4780 m). (**l**) Facies M3: (30/7a-7); ϕ, 10.5%; K_h, 0.11 mD; depth, 11 479 ft (3498.8 m). LEFC, low-energy fluvial channel; HEFC, high-energy fluvial channel; SF, splay/sheetflood; FL, floodplain/lake facies.

Diagenesis

Compaction

Skagerrak Formation sandstones exhibit different degrees of mechanical compaction, with minimal input from chemical compaction. Evidence of mechanical compaction in the studied sandstones include grain rearrangement, grain deformation, bending of mica grains (Fig. 10a), and point and long grain contacts between grains (Fig. 10b, c). Chemical compaction features include concave–convex and sutured grain contacts, and these occur between some detrital quartz grains (Fig. 10b, d). An important parameter for measuring the degree of mechanical compaction is intergranular volume (IGV), which is the sum of intergranular porosity, intergranular cement and depositional matrix (Houseknecht 1987, 1988; Paxton *et al.* 2002). The calculated IGV values range from 16.3 to 38.1% (average

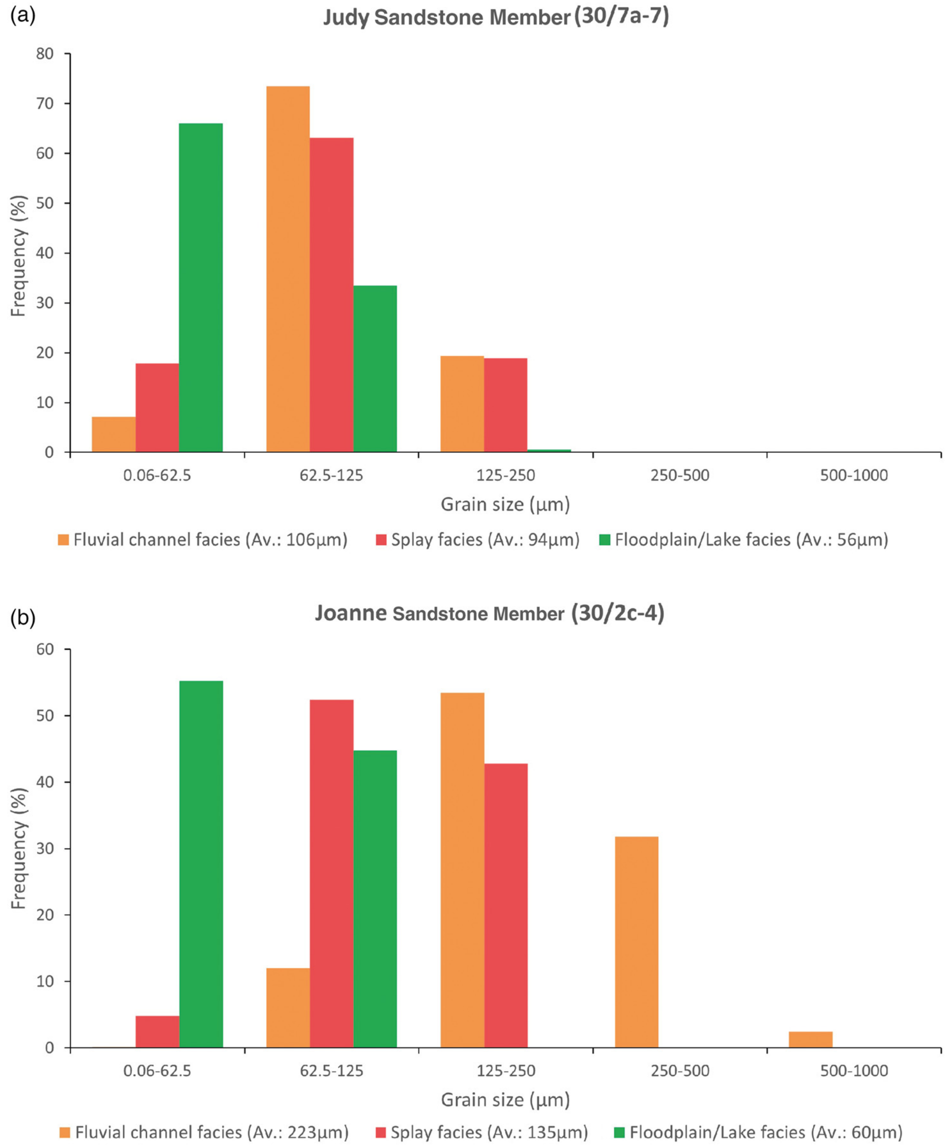

Fig. 8. Grain-size distribution by facies for (**a**) the Judy Sandstone Member and (**b**) the Joanne Sandstone Member. Av., average.

25.7%) and from 12.5 to 42.8% (average 28.4%) in wells 30/7a-7 and 30/2c-4, respectively (Table 6). The wide range in IGV values indicates variations in the degree of compaction between the samples. Cross-plots of COPL and CEPL for the studied sandstone samples are shown in Figure 10e, f. Sandstone samples with a clay matrix of >10% were not included in the cross-plots to avoid an overestimation of the compactional porosity loss due to abundant clay matrix (Lundegard 1992). In the Judy well (30/7a-7), the COPL and CEPL values range from 20.4 to 34.3% (average 27.8%) and from 3.8 to 13.8% (average 8%), respectively, while in the Jade well (30/2c-4), the COPL and CEPL values range from 11.9 to 37.1% (average 24.7%) and from 4.7 to 31.6% (average 11.6%), respectively (Table 6). In well 30/7a-7, 11% of the samples fall between the 0 and 10% intergranular porosity line, while the remaining 89% fall within the 10–20% intergranular porosity lines. In well 30/2c-4, 40% of the samples fall within the 0–10% intergranular porosity lines, 52% fall between the 10 and 20% lines, while the remaining 8% fall between the 20 and 30% intergranular porosity lines. The significance of the COPL v. CEPL plot is highlighted in the Discussion.

Diagenetic minerals

Quartz cement. In the studied sandstone samples, quartz cement occurs mainly as syntaxial quartz overgrowths on detrital quartz grains. They typically occur on non-clay-coated quartz-grain surfaces or at breaks within clay coatings. Where present, they partially or fully cover detrital quartz grains and encroach into the available pore spaces (Fig. 11a–d). Quartz cement thickness ranges from 2.3 to 100 μm with an average of 14 μm. Based on point counting, quartz cement volume ranges from 0.3 to 4.7% (average 1.7%) in the Judy Sandstone Member, and from 0.3 to 7.3% (average 3.2%) in the Joanne Sandstone Member (see the Supplementary material). Microquartz cement has been reported for the Skagerrak Formation sandstones (Nguyen *et al.* 2013; Stricker and Jones 2016) but was not observed in the analysed samples.

Clay minerals. Diagenetic clay minerals are common in all the sandstones studied. Detailed petrographic and SEM–EDX analysis revealed that the diagenetic clay minerals are predominantly chlorite and, to a lesser extent, a mixture of illite and chlorite (Figs 11d–j and 12). Kaolin was not observed in the studied samples. The diagenetic clays occur in variable amounts and in three principal forms: grain-coating, pore-filling and grain-replacing. The diagenetic grain-coating clays are mainly chlorite but in some samples they coexist with illite; they occur on the surfaces of the detrital grains (e.g. quartz and feldspar: Fig. 11a–h) and, in some instances, are enclosed by the pore-filling clays, making their identification challenging. The diagenetic pore-filling clays are mostly chlorite (Fig. 11i); however, a mixture of densely packed illite and chlorite,

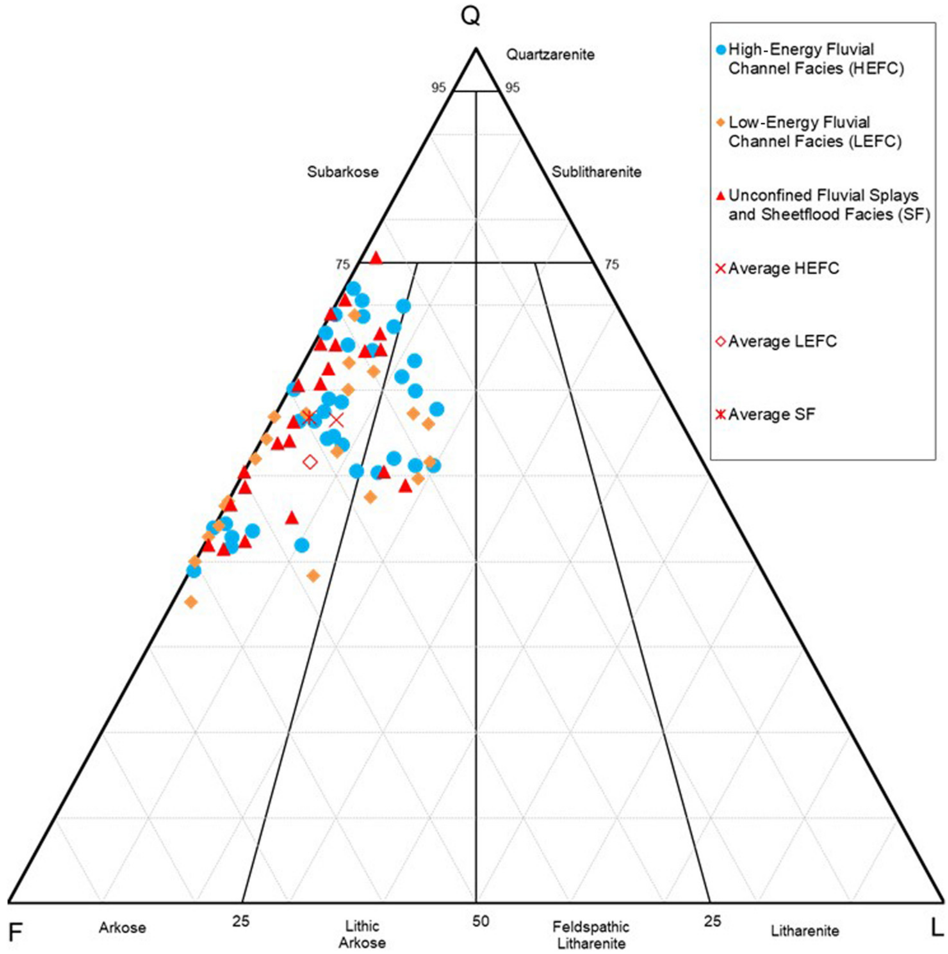

Fig. 9. QFL plot showing the classification of the Skagerrak Formation sandstones in this study (after Folk 1980).

occurring as pore-filling clay, is also observed in some samples (Fig. 11j).

Chlorite coat properties (coverage and thickness). As revealed by SEM–EDX analysis, the chlorite coats in the studied sandstones are Fe- and Mg-rich (Fig. 12; Table 7). In a few samples, the chlorite coats commonly display two layers, each exhibiting a different morphology and orientation (Pittman *et al.* 1992; Stricker and Jones 2016; Stricker *et al.* 2018). Layer 1 (or root zone) is made up of densely packed, laminated and poorly crystallized sheets, orientated parallel to the detrital quartz-grain surface (Fig. 12). Layer 2 (outer layer) contains well-defined crystals that are parallel but sometimes near perpendicular to the grain surface (Fig. 12). Layer 1 comprises a mixture of illite and chlorite, whereas layer 2 is mainly chlorite (Fig. 12). The chlorite coats are less developed and discontinuous on some grains but are well developed and continuous on others. Where they are absent or discontinuous, quartz overgrowth cements are observed (Fig. 11a–c). However, in samples where chlorite coats are well developed and continuous, the development of quartz overgrowth cements was inhibited (Fig. 11d–h). Chlorite coat coverage and thicknesses on the measured grains range from 1.2 to 100% and from 0.5 to 16 µm, respectively. Average chlorite coat coverage in the Joanne Sandstone Member samples ranges from 15.9 to 69%, with 69% of the samples having <40% average chlorite coat coverage. In the Judy Sandstone Member samples, the average chlorite coat coverage is higher, ranging from 70 to 98%; 98% of the coating thickness values are <10 µm, while the remaining 2% are within the range 10–16 µm. Coating thickness values >10 µm are commonly found in grain embayments (Fig. 11f, h). Average chlorite coat thickness ranges from 4.2 to 7.2 µm in the Joanne Sandstone Member samples, whereas it ranges from 3.5 to 6.2 µm in the Judy Sandstone Member samples. Coating thickness is generally not uniform on the grain surfaces; they are often thicker in grain embayments (i.e. grain indentations) (Fig. 11i). A summary of the chlorite coat coverage and thickness measurements is presented in Table 8.

Carbonate cement. Dolomite is the principal carbonate cement in the studied samples (Fig. 13a, b). Dolomite cements are found in all the facies identified; however, in variable amounts. Volumetrically, they range from 0 to 42.7%, with an average value of 11.1%. They are locally distributed and occur mainly as pore-filling and, in some cases, infilling in partly dissolved grains. Dolocrete clasts deposited simultaneously with mud intraclasts were also recognized but are restricted to channel bases (Fig. 7i, facies C). Petrographic and SEM–EDX analysis revealed two types of dolomite cements: non-ferroan (nFe-D) and ferroan dolomite (Fe-D) cements. Based on petrographic light microscopy analysis, the nFe-D shows no stain, while the Fe-D was identified by its characteristic pale turquoise blue stain with potassium ferricyanide (Fig. 13a). Both types exhibit a rhombic crystal structure with compositional zonation in some places. The ferroan dolomite cements were observed to enclose the non-ferroan phase (Fig. 13a, b), indicating that they formed during a later stage of diagenesis (i.e. mesodiagenesis).

Porosity and permeability distribution

Thin-section and helium porosity of samples from the Judy Sandstone Member (well 30/7a-7) range from 0 to 21% (average 7.3%) and from 2.3 to 26.7% (average 19.1%), respectively, while the Joanne Sandstone Member samples (well 30/2c-4) have thin-section and helium porosity values in the range 0–23.9% (average

Table 4. *Summary of petrographic data for the Skagerrak Judy sandstones in the Judy Field (well 30/7a-7) by facies*

Judy sandstones (30/7a-7)	LEFC				HEFC				SF			
	Min.	Max.	Average.	*N*	Min.	Max.	Average.	*N*	Min.	Max.	Average	*N*
Quartz (%)	20	45	33.8	22	30	42.7	35.3	8	25.7	44.7	33.2	12
Feldspar (%)	17.7	42.7	28.2	22	15	46.7	23.8	8	10.7	41.6	23.9	12
Total lithic fragments (%)	0.3	13.6	6.1	22	0.3	12.6	7.7	8	0.3	11	3.6	12
Total mica (%)	0.7	13.6	6	22	1.3	9.3	4.1	8	1.3	19.6	8	12
Quartz cement (%)	0.3	4.7	1.5	22	0.7	4.3	3.1	8	0	3.8	0.8	8
K-feldspar cement (%)	0	0.7	0.4	22	0	0.7	0.2	8				
Carbonate cement (%)	0	30	1.4	22	0	8.3	1.8	8	0.7			
Helium porosity (%)	2.3	26.7	22.3	22	17.9	26.0	23.8	8	6.9	23.5	17.5	12
Permeability (mD)	0.01	141	41.2	22	14.0	539	155.9	8	0.01	166	17.3	12
Grain size (mm)	0.07	0.13	0.09	22	0.12	0.17	0.14	8	0.07	0.14	0.09	12
Sorting (Folk and Ward)	0.30	0.61	0.38	22	0.36	0.43	0.38	8	0.32	0.45	0.39	12
Pore-filling clay (%)	0.7	32.7	6.8	22	0	19.6	3.9	8	0	37.6	18.9	12
Grain-coating clay (%)	0.3	17.4	7.5	22	2.7	8.3	5.8	8	0.3	9.7	5.4	12
Total clay (%)	6.3	33	14.3	22	5.6	22.3	9.7	8	6.6	46.9	24.2	12
Intergranular porosity (%)	0.3	13.6	8.4	22	2.4	17.0	9.7	8	0	18.7	4.2	12
Dissolution porosity (%)	0.3	5.6	2.3	22	1.0	6.0	3.7	8	0	5.0	1.4	12
Microporosity (%)	2.3	18.5	11.8	21	2.6	15	9.4	7	2.5	17.8	12.0	12
Total thin-section porosity (%)	0.3	16.6	10.2	22	6.1	19.4	13.4	8	0.7	21	5.5	12
IGV (%)	18.6	31.3	24.3	21	16.3	30.9	25.4	8	18.2	38.1	28.5	11

More detailed data are reported in the Supplementary material: Table S1.

5.1%) and 3.7–25.9% (average 13.7%), respectively. Core permeability ranges from 0.055 to 539 mD (average 40.9 mD) in the Judy Sandstone Member and from 0.004 to 1150 mD (average 197.4 mD) in the Joanne Sandstone Member (see the Supplementary material: Tables S1 and S2). Cross-plots of helium porosity and permeability show a strong positive correlation ($R = 0.9$) in both the sandstone members (Fig. 14a, b). The thin-section porosity also significantly correlates with permeability (Fig. 14c, d). Pore types identified in the studied samples include primary (intergranular), secondary (dissolution) and micropores, with intergranular pores dominating the pore system. Intergranular porosity ranges from 0.3 to 18.7% (average 7.8%) in the Judy sandstones and from 0 to 21.3% (average 8.8%) in the Joanne sandstones. Secondary porosity in the Judy and Joanne sandstones ranges from 0.3 to 6% (average 2.3%) and from 0 to 5.7% (average 1.7%), respectively. The secondary pores were created by partial to complete dissolution of detrital grains (feldspars and rock fragments) (Fig. 13c, d). The micropores are not visible under the microscope. They are associated with the clay minerals in the studied sandstone samples and are responsible for the higher helium

Table 5. *Summary of petrographic data for the Skagerrak Joanne sandstones in the Jade Field (well 30/2c-4) by facies*

Joanne sandstones (30/2c-4)	LEFC				HEFC				SF			
	Min.	Max.	Average	*N*	Min.	Max.	Average	*N*	Min.	Max.	Average	*N*
Quartz (%)					19.3	54.7	37.7	26	27.6	40	32.9	11
Feldspar (%)					6.3	39.3	24.5	26	12	42.3	23.7	11
Total lithic fragments (%)					0.3	11.7	3.4	26	0.3	3.6	1.4	11
Total mica (%)					0.3	8.3	2.5	26	0.3	6.3	3.0	11
Quartz cement (%)					0.3	7.3	3.8	26	0	4.3	0.9	11
K-feldspar cement (%)					0	1.3	0.2	26	0	0.3	0.1	11
Carbonate cement (%)					0	42.7	8.1	26	0	36.3	8.5	11
Helium porosity (%)					4.9	25.9	19.2	24	6.5	16.0	11.4	11
Permeability (mD)					0.038	1150	394.7	24	0.004	2.35	0.41	11
Grain size (mm)					0.13	0.33	0.21	26	0.063	0.19	0.12	11
Sorting (Folk and Ward)					0.36	0.71	0.5	26				
Pore-filling clay (%)					0	27.9	2.9	26	3.6	33.6	23.3	11
Grain-coating clay (%)					0.3	8.3	3.5	26	0.7	7.0	3.8	11
Total clay (%)					1.3	29.2	6.4	26	7.6	36.2	27.1	11
Intergranular porosity (%)					0	21.3	9.3	26	0	3.0	0.7	11
Dissolution porosity (%)					0	5.7	1.9	26	0	2.0	0.7	11
Microporosity (%)					1.4	19.8	7.4	24	6.5	15.7	10.1	11
Total thin-section porosity (%)					0	23.9	11.2	26	0	4.3	1.4	11
IGV (%)					16.9	37.6	27.1	24	12.5	42.8	32.3	8

More detailed data are reported in the Supplementary material: Table S2.

Table 6. *Distribution of grain size, porosity, permeability and other measured parameters for the Judy and Joanne sandstones in wells 30/7a-7 (Judy Field) and 30/2c-4 (Jade Field)*

Formation/well		Grain size (mm)	Thin-section porosity (%)	Helium porosity (%)	Permeability (mD)	Total clay (%)	Pore-filling clay (%)	Grain-coating clay (%)	Microporosity (%)	IGV (%)	COPL (%)	CEPL (%)
Judy sandstones (30/7a-7)	Minimum	0.065	0	2.3	0.01	5.6	0	0.3	2.3	16.3	20.4	3.8
	Maximum	0.165	21.0	26.7	539.0	46.9	37.6	17.4	18.5	38.1	34.3	13.8
	Average	0.102	9.5	21.1	54.1	16.2	9.7	6.6	11.4	25.7	27.8	8.0
Joanne sandstones (30/ 2c-4)	Minimum	0.063	0	4.9	0.004	1.3	0	0.3	1.4	12.5	11.9	4.7
	Maximum	0.33	23.9	25.9	1150	36.2	33.6	8.3	19.8	42.8	37.1	31.6
	Average	0.19	8.3	16.8	270.8	12.5	8.9	3.6	8.3	28.4	24.7	11.6

porosities compared to the thin-section porosities (Fig. 14e, f). Microporosity ranges from 2.3 to 18.5% (average 11.4%) in the Judy sandstones and from 1.4 to 19.8% (average 8.3%) in the Joanne sandstones (Tables 4 and 5). Cross-plots of microporosity against total clay and grain-coating clay estimated from point counting show that microporosity generally increases with increasing clay content (Fig. 14g, h).

Discussion

Facies/depositional control on reservoir quality

Reservoir quality (i.e. porosity and permeability) of the Triassic Skagerrak Formation is primarily controlled by depositional processes, facies, grain size and clay content (Figs 14 and 15). The best-quality reservoirs are associated with fluvial channel facies (HEFC and LEFC); however, some splay facies (SF) also retain good reservoir quality. Lacustrine and floodplain facies (FL) constitute non-reservoirs; although they have 5–18.9% helium porosity (Fig. 14a, b), permeability is less than 1 mD and could thus act as barriers or baffles to fluid flow. Within the channel facies, HEFC sandstones have better reservoir quality (in terms of permeability) than the LEFC sandstones (Fig. 14a, b). Cross-plots of petrographic data show that the main facies elements controlling reservoir-quality distribution are grain size and clay content, both of which are influenced by depositional processes (Fig. 15).

The impact of grain size on the porosity and permeability of the studied Skagerrak Formation sandstones is shown in Figure 15a–f. As grain size increases, there is a general increase in porosity (thin section and helium) and permeability in the Judy and Joanne sandstones. With the exception of a few isolated points, permeability values in the range of 100–1150 mD are generally restricted to the fine- to medium-grained HEFC sandstones with an average grain size of >0.15 mm (lower fine sand to lower medium sand), while permeability values of <100 mD are restricted to the very-fine-grained LEFC sandstones and very-fine- to fine-grained SF sandstones with an average grain size of <0.15 mm (lower very fine sand to lower fine sand) (Fig. 15e, f). Furthermore, cross-plots of grain size and calculated permeability using the Kozeny equation (Kozeny 1927; Walderhaug *et al.* 2012) show a significant positive correlation, with calculated permeability increasing as grain size increases (Fig. 15g, h). Although the Kozeny equation over-estimates permeability for most of the samples (see the Supplementary material: Tables S4 and S5), it does demonstrate that grain size has a strong influence on permeability. The HEFC sandstones, on average, are coarser grained (upper fine sand), whereas the LEFC sandstones are, on average, finer grained (upper very fine sand). An important parameter controlling permeability is pore-throat size, which is a function of grain size (Bloch *et al.* 2002; Nelson 2009; Lala and El-Sayed 2017; Lai *et al.* 2018). In this study, higher permeability in the fine- to medium-grained HEFC sandstones is associated with larger pore-throat sizes, while lower permeability in the very-fine-grained LEFC and SF sandstones is associated with smaller pore-throat sizes (Fig. 7a–c).

The impact of clay content on the reservoir quality of the investigated Skagerrak Formation sandstones (channel and splay/sheetflood) is shown in Figure 15i–k. The figure shows an inverse correlation between clay content and porosity–permeability. As clay content increases, there is a general decrease in porosity and permeability. In this study, sandstones with <16% total clay generally have better reservoir quality (>10 mD), while those with >16% total clay have lower to poor reservoir quality (<10 mD) (Fig. 15k). According to Worden and Morad (2003), the amount, distribution pattern and morphology of clay minerals have significant impacts on the porosity and permeability of sandstones. Clay minerals in the form of grain coats (Fig. 11d–h) can preserve porosity by preventing the development of quartz overgrowths (Walderhaug 1996; Stricker and Jones 2016; Tang *et al.* 2018*a*). Pore-filling clays (Fig. 11i, j), on the other hand, can degrade reservoir quality by enhancing mechanical compaction and blocking pore throats (Schmid *et al.* 2004; Olivarius *et al.* 2015; Oluwadebi *et al.* 2018; Barshep and Worden 2021; Bello *et al.* 2021; Bukar *et al.* 2021). In this study, porosity and permeability decrease with increasing volume of pore-filling clay (see the Supplementary material: Figs S2–S4). Generally, sandstones with >9% pore-filling clay have lower permeabilities (<10 mD), while those with <9% pore-filling clay have higher permeabilities (>10 mD).

The variations in sand grain size and clay content between/within the channel (i.e. HEFC and LEFC) and splay/sheetflood facies associations could be attributed to variations in depositional energy. The very-fine-grained, clay-rich LEFC sandstones are suggestive of deposition in a lower-energy environment, while the fine- to medium-grained, relatively clean HEFC sandstones are suggestive of deposition in a higher-energy environment. Our study shows that as you move from a high-energy environment to a low-energy environment there is a general decrease in grain size and an overall increase in clay content (Fig. 15l), and, hence, an overall reduction in reservoir quality. The ratio of HEFC/LEFC sandstones varies between the Joanne and Judy sandstone members. In the Joanne Sandstone Member, the fluvial channel facies are predominantly HEFCs. In the Judy Sandstone Member, 15% of the fluvial channels are HEFCs, while the remaining 85% are LEFCs. In general, channel sandstones from the Joanne Sandstone Member have better permeabilities (up to 1150 mD) due to their coarser grain size (fine–medium grained) and lower total clay content (average 6.4%), which are related to their higher depositional energy. Conversely, channel sandstones from the Judy Sandstone Member have lower permeabilities due to their finer grain size (very fine grained) and higher clay content (average 13.1%), which are indicative of their lower depositional energy. The above findings are similar to those of previous research in the Judy and Jade fields, where depositional facies has been identified as the primary control on reservoir quality (Jones *et al.* 2005; Keller *et al.* 2005).

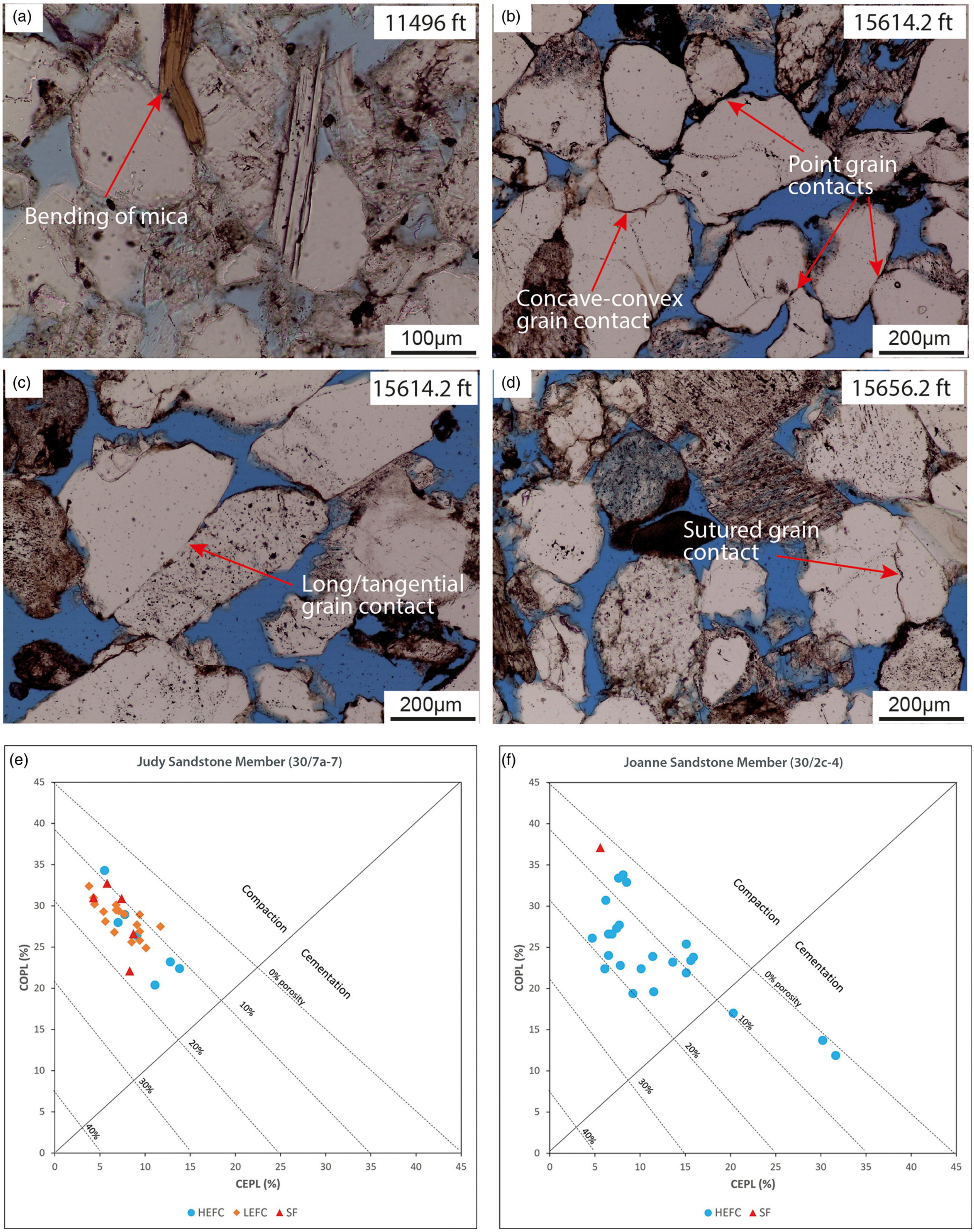

Fig. 10. Thin-section photomicrographs showing (**a**)–(**d**) different compaction features and (**e**) and (**f**) plots of porosity loss due to compaction (COPL) and cementation (CEPL). (**a**) Bending of mica; (**b**) point and concave–convex grain contacts; (**c**) long grain contact; (**d**) sutured grain contact; and (**e**) and (**f**) plots of COPL and CEPL for low-energy fluvial channel (LEFC), high-energy fluvial channel (HEFC) and splay facies (SF) in the Judy and Joanne sandstone members. Sandstone samples with more than 10% clay matrix were not included to avoid an overestimation of compactional porosity loss.

Diagenesis and reservoir quality evolution

During burial diagenesis, compaction and cementation are the two main processes reducing reservoir quality (Houseknecht 1987; Gluyas and Cade 1997; Wolela and Gierlowski-Kordesch 2007; Tang *et al.* 2018*b*). Cross-plots of porosity loss due to compaction (COPL) and cementation (CEPL) show that porosity loss in the majority of studied sandstones is mainly due to compaction

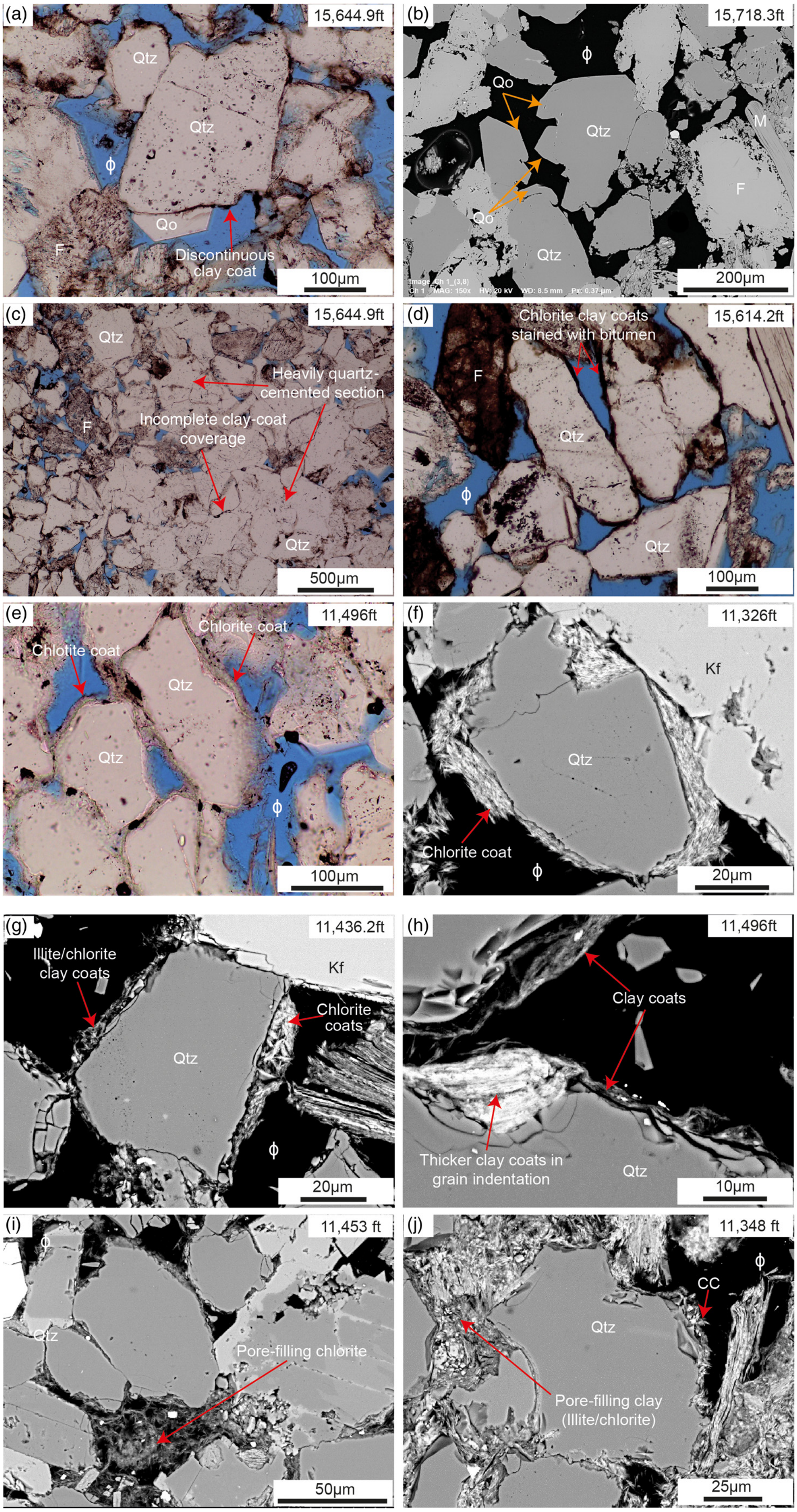

Fig. 11. Thin-section photomicrographs and BSE images showing detrital quartz (Qtz), feldspar (F), mica (M), quartz overgrowth (Qo), clay coats, pore-filling clays and porosity (ϕ). (**a**)–(**c**) Thin-section photomicrographs showing quartz overgrowth (Qo) and discontinuous clay coats on detrital quartz grains; (**d**) and (**e**) thin-section photomicrographs showing well-developed and continuous clay coats; (**f**) and (**g**) BSE images showing well-developed clay coats; (**h**) BSE image showing thicker clay coats in grain indentation; and (**i**) and (**j**) pore-filling clays occluding pore space.

(Fig. 10e, f). However, a few HEFC data points in Figure 10f suggest that cementation also plays a significant role in porosity loss. These data points (or samples) are mainly from channel bases and pedoturbated sandstones with significant amounts of dolomite cement (10–42.7%). Based on petrographic textural observations, compaction is primarily mechanical and largely influenced by

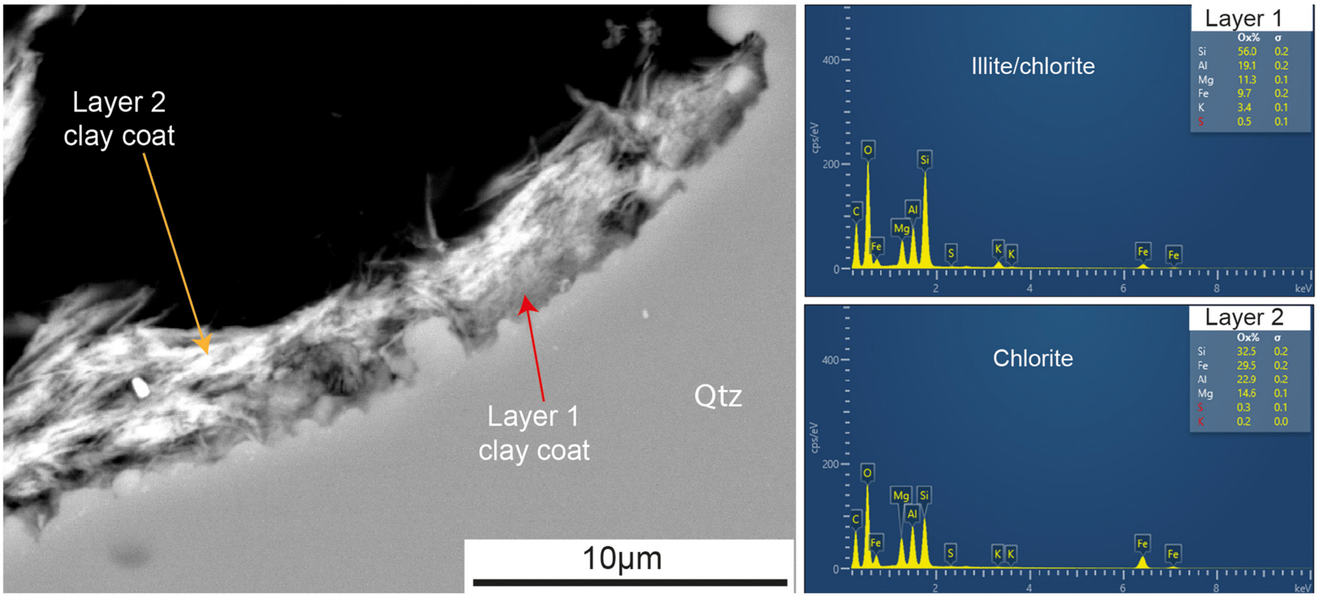

Fig. 12. BSE image and EDX spectra of a sample at 11 348 ft (well 30/7a-7) showing a two-layered clay coats. The EDX spectra on the right show changes in the clay coat chemistry from the root zone to the outer layer. The root zone (layer 1) is a mixture of illite and chlorite, while layer 2 is pure chlorite.

depositional facies. According to Paxton *et al.* (2002), sandstones with a high proportion of ductile grains, such as mudclasts or mica, exhibit significantly higher levels of porosity loss by mechanical compaction at relatively shallow depths of burial. In this study, channel sandstones (HEFC and LEFC) have a relatively lower degree of compaction (Fig. 7a–c) due to the absence or lesser amount of detrital clay and mica. Unconfined splay/sheetflood (SF) sandstones have a greater degree of compaction (Fig. 7f) due to larger amounts of detrital clay and mica content. Very few SF sandstone samples were observed to have undergone lesser compaction due to minimal amounts of clay/mica, thus retaining good porosity and moderate permeability (Fig. 7e). In addition to depositional facies exerting a significant influence on the variations in the compaction state, several studies have identified low vertical effective stress (VES) as a critical factor for reduced state of compaction and reservoir quality preservation (Grant *et al.* 2014; Stricker *et al.* 2016*a*).

Apart from carbonate cements, other important diagenetic cements in the studied sandstones are chlorite, a mixture of chlorite and illite, and quartz. The diagenetic clays occur mainly as pore-filling and coatings, and predate quartz cements. Where they occur as pore-filling, pore spaces and pore throats are occluded, thus reducing reservoir quality (Fig. 11i, j). In contrast, where they occur as coatings (mainly chlorite), quartz cementation is inhibited and porosity is preserved (Fig. 11d–h). Quartz cement is variable (generally <8%) and localized (Fig. 11c), and has had minimal or no effect on the overall porosity and permeability due to the inhibiting effect of pore-filling clays and chlorite clay coats (Figs 11d–j and 12).

Clay coats and reservoir quality

Origin of chlorite coats

The chlorite coats in the studied Skagerrak Formation sandstones, as revealed by SEM analysis, are mostly orientated parallel to detrital grain surfaces (Fig. 11f–h), indicating a detrital origin and emplacement by mechanical infiltration process (Matlack *et al.* 1989; Pittman *et al.* 1992). In addition, the presence of thicker chlorite coats within the embayments on detrital grain surfaces (Fig. 11h) and wide variations in rim thickness point to a detrital origin (Pittman *et al.* 1992; Wilson 1992). Several studies have shown that chlorite-coat formation in sandstones takes place during diagenesis through precursor phases such as berthierine, odinite, kaolinite and smectite (Moraes and De Ros 1992; McKinley *et al.* 2003; Dowey *et al.* 2012; Charlaftis *et al.* 2021). As revealed by SEM–EDX analysis, the chlorite coats in the studied sandstones are Fe- and Mg-rich (Fig. 12; Table 4), suggesting a detrital smectite precursor clay mineral. This agrees with earlier interpretations where chlorite coats in the Skagerrak sandstones have been interpreted to form by thermally driven recrystallization of precursor detrital smectite coats (Stricker *et al.* 2016*b*). The recrystallization of smectite to chlorite occurs via a mixed-layer chlorite–smectite at around 120°C (Worden and Morad 2003; Worden *et al.* 2020). The present-day reservoir temperature of the studied Skagerrak sandstones is >160°C (Fig. 3). This implies that any smectite precursor clays would have been fully recrystallized to chlorite at this temperature. As earlier mentioned, the clay coatings on some of the detrital quartz grains exhibit two layers: an inner layer (layer 1/root zone) and an outer layer (layer 2) (Fig. 12). As shown in

Table 7. *Result of a spot SEM–EDX spectral analysis conducted on a two-layered clay coat on a detrital quartz grain (shown in Fig. 12)*

	Layer 1		Layer 2	
	Wt (%)	Oxide (%)	Wt (%)	Oxide (%)
Elements				
O	42.7		40.7	
Si	26.3		15.3	
Al	13.7		12.2	
Fe	7.6		22.9	
Mg	6.9		8.9	
K	2.8		0	
Total	100		100	
Oxides				
SiO_2		56.3		32.7
Al_2O_3		19.2		23.1
FeO		9.7		29.5
MgO		11.4		14.7
K_2O		3.4		0
Total		100		100
Clay type	**Illite–chlorite**		**Chlorite**	

Table 8. *Summary of clay-coat coverage measurements made on 23 sandstone samples from the Skagerrak Formation*

Well name	Sandstone Member	Depth (ft)	Facies	Average grain size (mm)	Sorting	Clay-coat coverage (%)	Clay-coat volume_point count (%)	Total clay volume_point count (%)	Clay-coat thickness (μm)	Quartz cement volume (%)	Temperature (°C)	Thin-section porosity (%)	Helium porosity (%)	Permeability (mD)
30/07a-7	Judy	11 291.3	LEFC	0.098	0.44	78.5	7.3	11.1	3.7	1.8	164.0	9.7	24.1	43
30/07a-7	Judy	11 303.8	LEFC	0.089	0.40	95.3	10	11.3	6.2	1.6	164.0	12	25.7	18
30/07a-7	Judy	11 309.8	LEFC	0.093	0.44	96	6	9	4.9	0.5	164.0	14.4	21.5	27
30/07a-7	Judy	11 335.1	LEFC	0.092	0.38	93	6.7	10.3	3.5	1.7	164.0	14	25.7	45
30/07a-7	Judy	11 338.4	LEFC	0.097	0.34	91	5	7.6	4.9	1.3	164.0	13.3	26.2	53
30/07a-7	Judy	11 433	SF	0.097	0.37	82	8	10.7	3.6	4.7	164.0	13.7	25	48
30/07a-7	Judy	11 442	LEFC	0.101	0.40	98	5.6	6.3	5	2.7	164.0	14.7	25.9	85
30/07a-7	Judy	11 468.3	SF	0.144	0.42	70	7	6.6	4.5	3.8	164.0	21	23.5	166
30/07a-7	Judy	11 490.9	LEFC	0.135	0.50	92.7	5.2	6.3	4.7	4.2	164.0	16.6	21.9	52
30/07a-7	Judy	11 496	HEFC	0.145	0.40	80.4	8.3	8.3	5	4	164.0	19.4	25.3	269
30/02c-4	Joanne	15 612	HEFC	0.152	0.51	69	6.3	6.3	4.5	2.3	187.7	13	23.3	124
30/02c-4	Joanne	15 614.2	HEFC	0.259	0.56	50	4.8	5.5	4.6	6	187.7	21	25.4	890
30/02c-4	Joanne	15 617.1	HEFC	0.245	0.59	36.2	2.3	2.3	5.9	5	187.7	20.3	22	692
30/02c-4	Joanne	15 621.1	HEFC	0.32	0.60	30.2	1.7	2.3	5	4.3	187.7	19.7	23.4	842
30/02c-4	Joanne	15 625	HEFC	0.245	0.71	40	3.7	5.3	6.6	6	187.7	14.3	19.9	355
30/02c-4	Joanne	15 644.9	HEFC	0.22	0.44	60	5.3	6	7.2	4.5	187.7	19.6	24.4	670
30/02c-4	Joanne	15 650.1	HEFC	0.216	0.59	17	2.3	2.6	4.2	7.3	187.7	16.7	19.9	279
30/02c-4	Joanne	15 656.2	HEFC	0.211	0.55	36.8	3.3	3.3	6	4.2	187.7	23.9	25.3	1150
30/02c-4	Joanne	15 660	HEFC	0.221	0.52	27	1.3	1.3	6.2	6.2	187.7	19.7	23	1050
30/02c-4	Joanne	15 671	HEFC	0.145	0.60	60.2	8.3	8.3	5.3	2.7	187.7	13.7	25.9	167
30/02c-4	Joanne	15 676.2	HEFC	0.163	0.64	36	2.7	4.7	5.2	6.3	187.7	17.7	23.3	529
30/02c-4	Joanne	15 718.3	HEFC	0.183	0.55	17.3	2.7	3	5.3	6	187.7	21.1	24.7	614
30/02c-4	Joanne	15 748.2	HEFC	0.274	0.64	15.9	4	4.3	4.9	7	187.7	20	23	1134

Also included are measured textural parameters, quartz cement and clay-coat volume derived from point counting, and their corresponding reservoir properties (LEFC, low-energy fluvial channel; HEFC, high-energy fluvial channel; SF, unconfined splay sandstone facies).

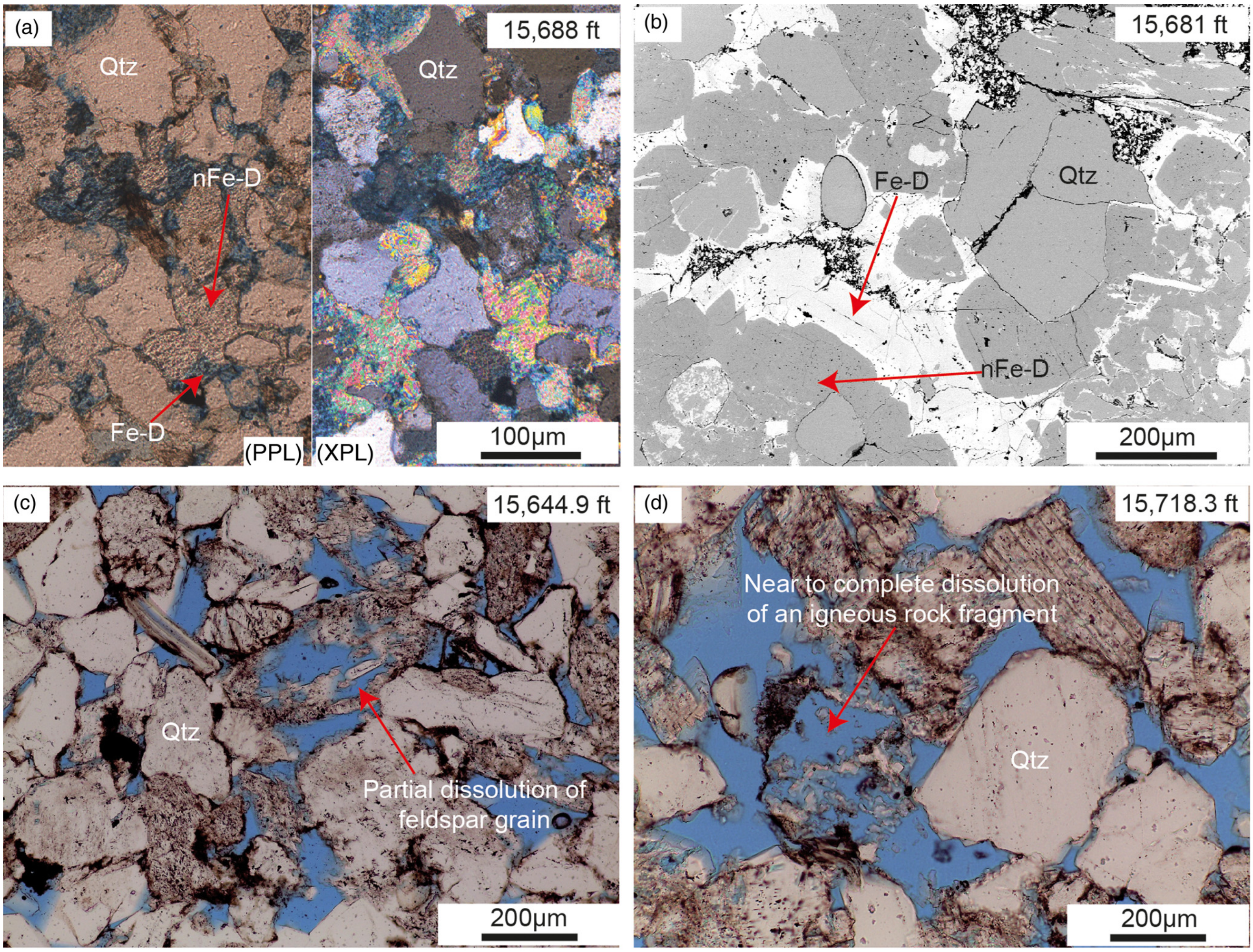

Fig. 13. (**a**) Thin-section photomicrograph showing non-ferroan (nFe-D) and ferroan dolomite (Fe-D) under plane-polarized (PPL) and cross-polarized light (XPL). (**b**) BSE image showing non-ferroan (nFe-D) and ferroan dolomite (Fe-D). Both dolomite types exhibit a rhombic crystal structure with compositional zonation. The ferroan dolomite encloses the non-ferroan phase, indicating that the ferroan dolomite was formed during late-stage diagenesis. (**c**) and (**d**) Thin-section photomicrographs showing secondary porosity created by partial and near to complete dissolution of feldspar grain (c) and igneous rock fragment (d).

Figure 12, the root zone directly overlying the detrital quartz-grain surface is densely packed, poorly crystallized, and composed of a mixture of illite and chlorite, which we believe is the product of the diagenetic recrystallization of detrital smectite coats. The presence of potassium in the root zone or layer 1 suggests the presence of small amounts of illite or mica as a contaminant within the chlorite structure (Humphreys *et al.* 1994; Shelukhina *et al.* 2021). The outer layer is well crystalized and purely chlorite. We hypothesize that the outer layer is younger and was formed by the interaction of the root zone's outermost part with adjacent porewaters during burial (due to increasing temperature and pressure); hence, the reason for changes in the chemistry and increased crystallinity of the clay coats from the root zone to the outer layer.

Smectite minerals preferentially form during weathering in arid climates (McKinley *et al.* 2003). In arid environments, evaporation frequently exceeds meteoric influx, resulting in an upward flow of groundwater, evaporation, and the formation of various smectitic clays and magnesium-rich clay minerals (Worden and Morad 2003). The Skagerrak Formation sandstones were deposited in an arid to semi-arid environment (McKie 2011, 2014), therefore supporting the assumption that the precursor clay mineral for the chlorite coats is smectite. In addition to smectite acting as a precursor for chlorite in the studied sandstones, the dissolution of volcanic rock fragments (Fig. 13d) observed in some samples may have aided the formation of chlorite. According to Dowey *et al.* (2012), authigenic chlorite can also form during diagenesis from the dissolution of Fe- and Mg-rich detrital grains and volcanic rock fragments. Thus, this observation is likely to support the interpretations of Humphreys *et al.* (1989) that authigenic chlorite in late Triassic sandstones from the North Sea Central Graben developed from a potential smectite precursor and was aided by detrital grain dissolution.

Chlorite coats and quartz cementation

Quartz cementation is the dominant mechanism for porosity loss in deeply buried sandstones, especially those with prolonged exposure to elevated temperatures (Worden and Morad 2000; Taylor *et al.* 2010; Xia *et al.* 2020). In this study, the modelled burial–thermal history (Fig. 3) reveals that the Triassic Skagerrak Formation is at its maximum burial depth (>3400 m) and temperature (>160°C) at the present day. Considering the temperature history, quartz cement, which commonly forms at around 70–80°C (Walderhaug 2000; Worden and Morad 2000; Bjørlykke 2014; Xi *et al.* 2015), is expected to have pervasively developed in the studied samples, occluding the entire pore spaces. However, this is not the case, as the quartz cement volume recorded is generally <8%. Petrographic examination reveals that the presence of early formed chlorite coats has significantly inhibited the growth of quartz cement and therefore

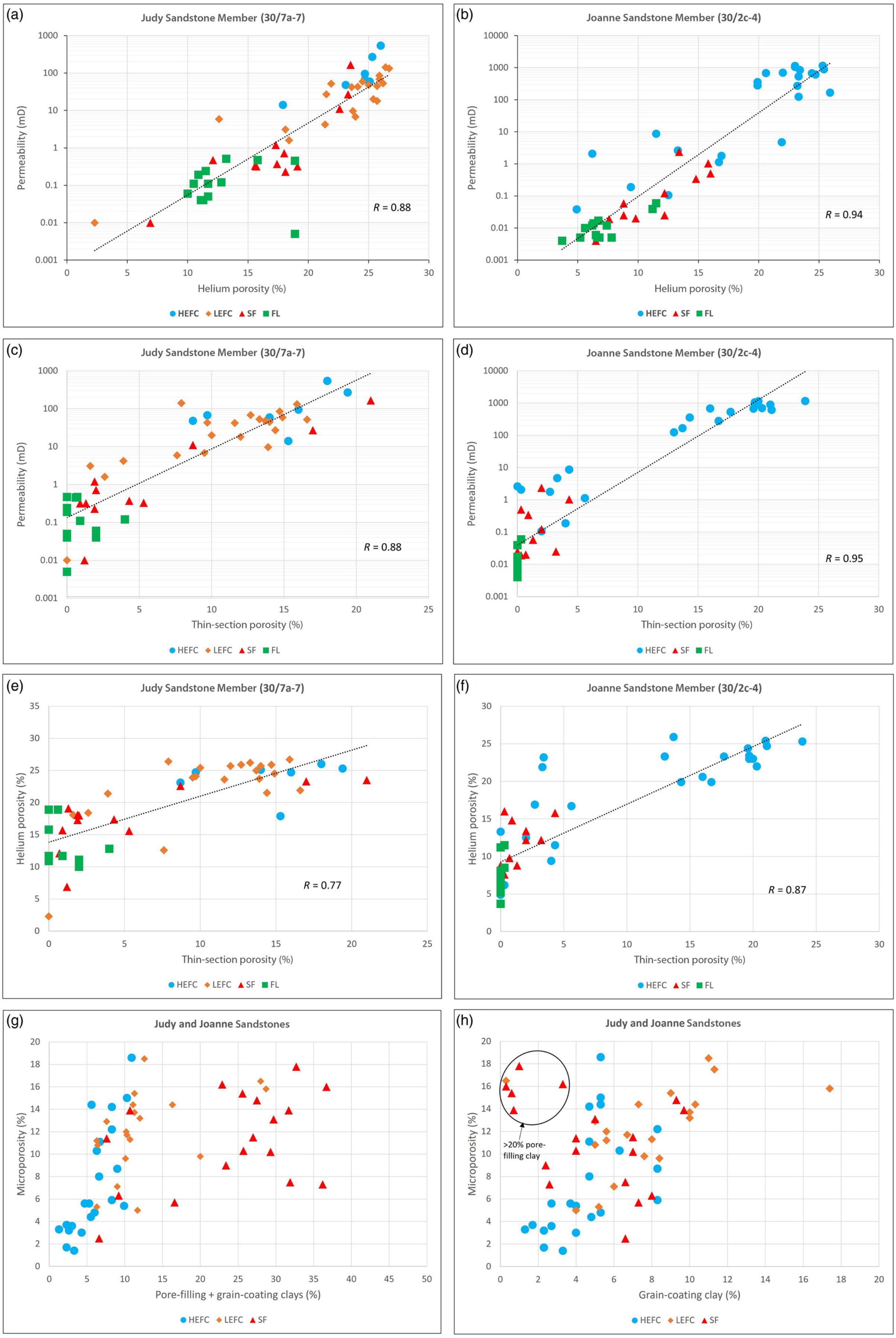

Fig. 14. (**a**) and (**b**) Cross-plots of helium porosity and permeability for the Judy and Joanne sandstones. (**c**) and (**d**) Cross-plots of thin-section porosity and permeability. (**e**) and (**f**) Cross-plots of helium porosity and thin-section porosity. (**g**) Cross-plots of clay microporosity and total clay (pore-filling and grain-coating clays). (**h**) Cross-plots of clay microporosity and grain-coating clay.

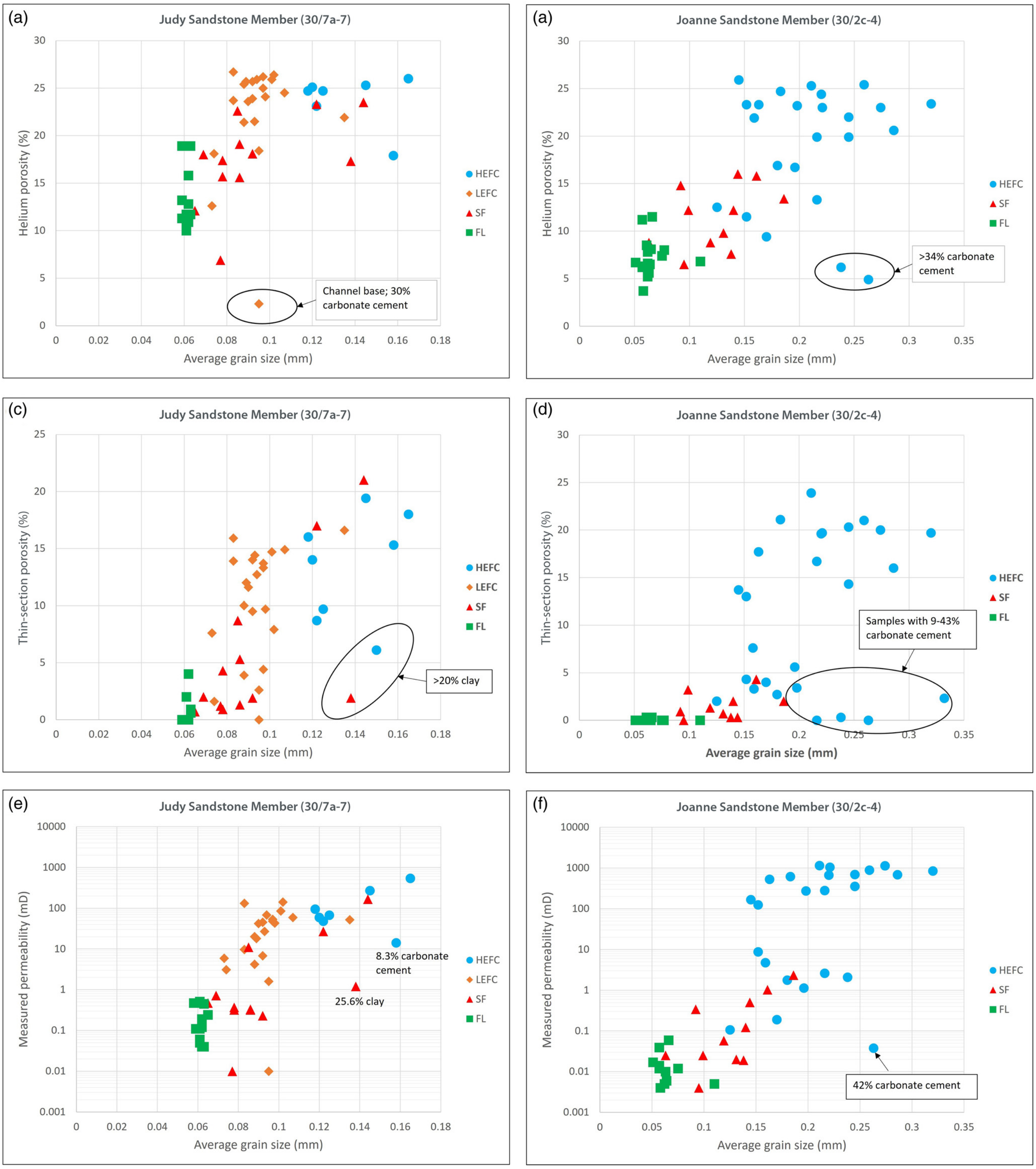

Fig. 15. Relationship between grain size, clay content and reservoir properties of the studied Skagerrak sandstones (HEFC, high-energy fluvial channel sandstones; LEFC, low-energy fluvial channel sandstones; SF, splay facies). (**a**) and (**b**) Cross-plots of helium porosity and average grain size. (**c**) and (**d**) Cross-plots of thin-section porosity and average grain size. The cross-plots show that porosity increases with increasing grain size. (**e**) and (**f**) Cross-plots of measured permeability and average grain size. (**g**) and (**h**) Cross-plots of Kozeny permeability (calculated) and average grain size for the Judy and Joanne sandstones. The cross-plots show that permeability generally increases with increasing grain size. (**i**) Cross-plot of helium porosity and total clay. (**j**) Cross-plot of thin-section porosity and total clay. The cross-plots show that porosity decreases with increasing total clay. (**k**) Cross-plot of measured permeability and total clay. Permeability decreases with increasing total clay. With few exceptions, sandstones with <16% total clay (circled) have better reservoir quality. (**l**) Cross-plot of total clay and average grain size. An increase in grain size results in a decrease in total clay.

contributed to the preservation of reservoir quality (Fig. 11d–h). However, in a few samples, quartz cementation is observed to be pervasive and locally distributed due to the absence or lack of continuous chlorite coats (Fig. 11a–c). In the studied sandstones, detrital quartz grains with continuous chlorite coats have minimal or no quartz cements, while those with discontinuous or no chlorite coats have moderate quartz cements. This implies that sandstones with discontinuous clay coats on detrital quartz grain surfaces are more prone to quartz cementation. Figure 16a shows the relationship between chlorite coat coverage (i.e. continuity/discontinuity) and

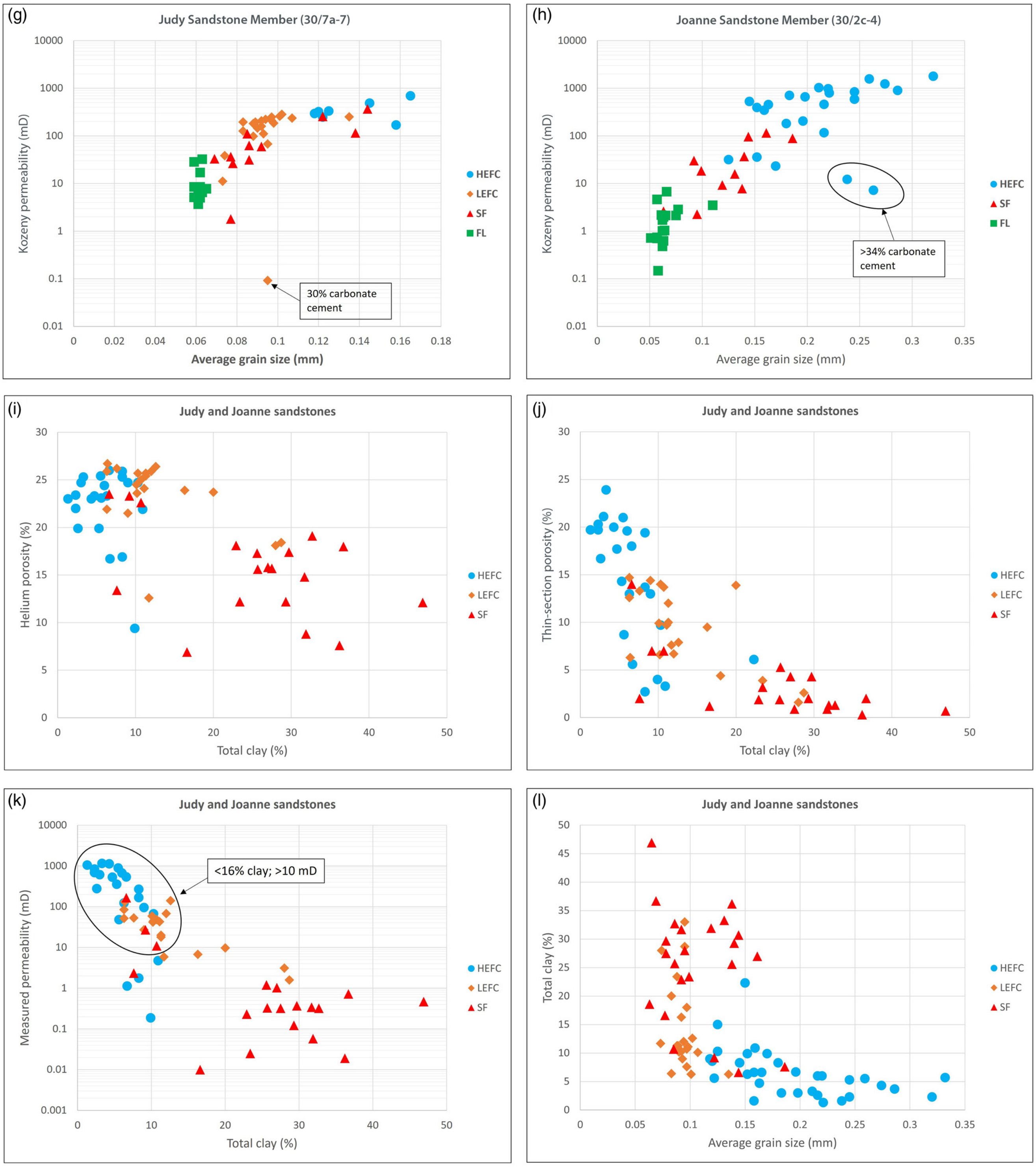

Fig. 15. Continued.

quartz cement volume for 23 of the investigated samples. As illustrated in Figure 16a, there is an inverse relationship between chlorite coat coverage and quartz cement, with quartz cement volume generally increasing as chlorite coat coverage decreases. With few exceptions, sandstones with a lower average chlorite coat coverage (<50%) have a higher quartz cement volume (4.2–7.3%), while those with a higher average chlorite coat coverage ranging from 60 to 98% have a lesser quartz cement volume (0.5–4.2%). This finding is similar to those of previous studies where an inverse correlation between clay-coat coverage and quartz cement volume has been identified (Bloch *et al.* 2002; Taylor *et al.* 2015; Dutton *et al.* 2018). In addition, this finding supports the claim that the completeness of clay coats and not just its presence is the most important factor governing its ability to effectively inhibit quartz cementation (Heald and Larese 1974; Ehrenberg 1993; Walderhaug 1996; Bloch *et al.* 2002; Billault *et al.* 2003; Lander *et al.* 2008; Ajdukiewicz and Larese 2012).

To further test the impact of the continuity or discontinuity of clay coats on quartz cementation and reservoir quality, clay-coat coverage data for 21 fluvial channel sandstone samples (Table 5) was incorporated into the quartz cementation model developed for this study (Fig. 16b, c). The sandstones of the Judy and Joanne

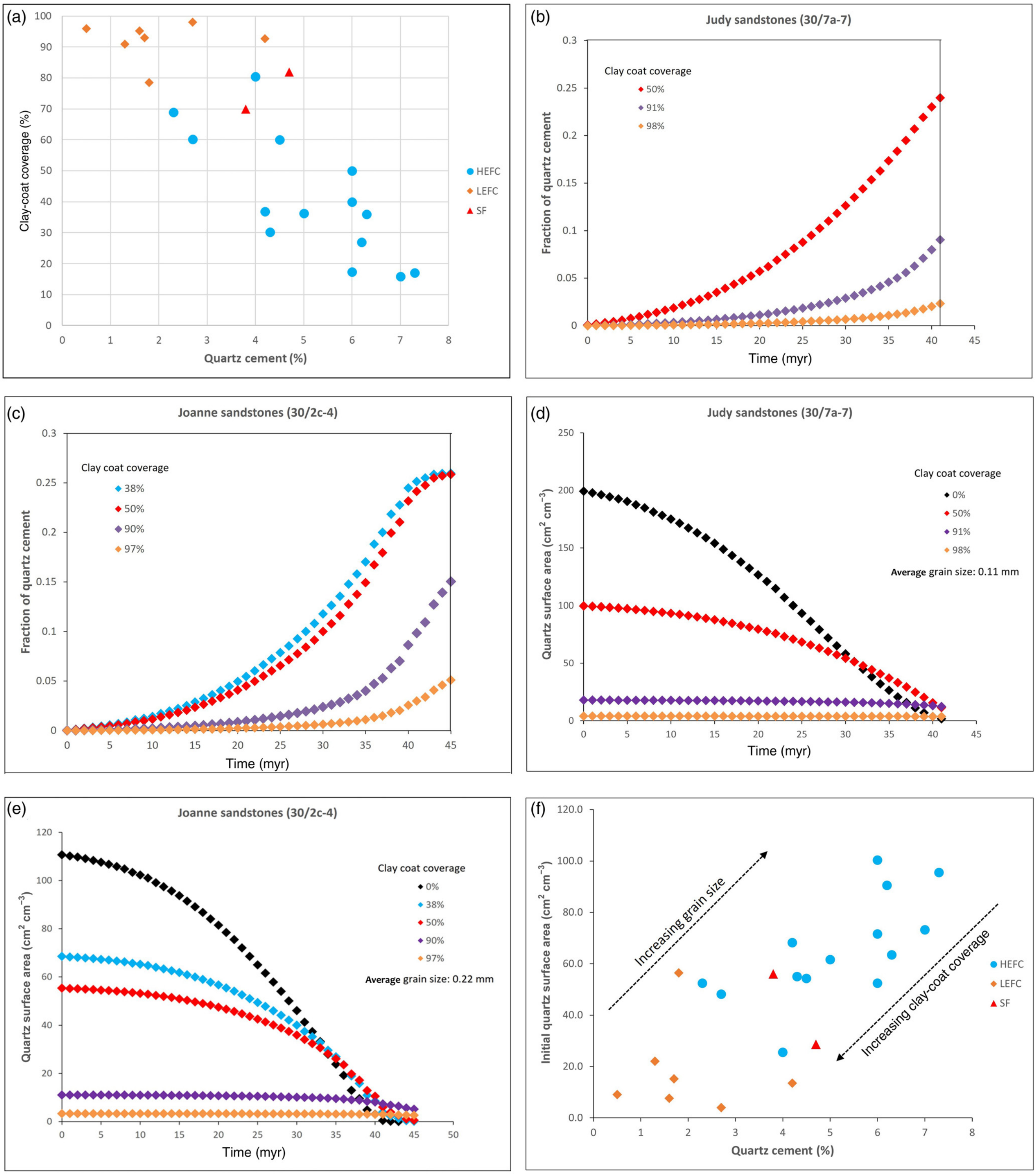

Fig. 16. (**a**) Inverse relationship between clay-coat coverage and quartz cement volume. (**b**) and (**c**) Quartz cementation model output for the Judy sandstones (Judy Field) and Joanne sandstones (Jade Field) showing the effect of varying clay-coat coverage on quartz cement evolution through geological time. Increasing clay-coat coverage results in a reduction of the quartz cement volume. Average measured clay-coat coverage in the Judy and Joanne sandstones is 91 and 38%, respectively. The model outputs indicate that the Judy and Joanne sandstones would require around 97–98% clay-coat coverage for their current average quartz cement volumes of 2.2 and 5.2%, respectively. (**d**) and (**e**) Quartz surface area v. time for the Judy and Joanne sandstones. The plots show the effect of varying the clay-coat coverage on the quartz surface area and its evolution through time. Generally, increasing clay-coat coverage results in a reduction of the initial quartz surface area available for quartz cement precipitation. (**f**) Cross-plot of point-counted quartz cement and initial quartz surface area per cubic centimetre of sandstone. The positive correlation suggests that the available quartz surface area (and the extent of the clay-coat coverage) have a significant influence on quartz cementation.

members are currently buried to temperatures of >160°C and have stayed in the quartz cementation window (above 80°C) for about 41 and 45 myr, respectively (Fig. 3). The model shows that with 50% clay-coat coverage in both the Judy and Joanne sandstone members, there is minimal or no effect on quartz cementation; however, increasing the clay-coat coverage to 90% results in a significant impact on quartz cementation. At 90–91% clay-coat coverage, the modelled quartz cement volume is 9.1% (after 41 myr in the quartz

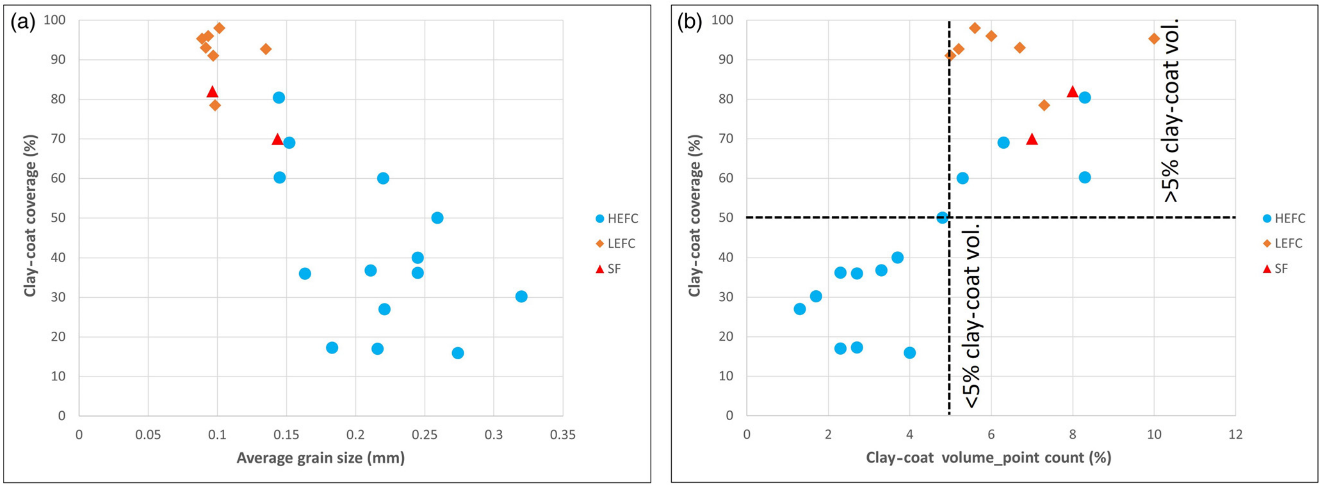

Fig. 17. (**a**) Correlation between clay-coat coverage and grain size. Clay-coat coverage increases with decreasing grain size and is influenced by depositional energy. Low-energy fluvial channel (LEFC) sandstones have better clay-coat coverage than their high-energy fluvial channel (HEFC) sandstone counterparts. (**b**) A positive correlation between clay-coat coverage and clay-coat volume. Clay-coat coverage increases with increasing clay-coat volume.

cementation window) and 15% (after 45 myr in the quartz cementation window) for the Judy and Joanne channel sandstones, respectively (Fig. 16b, c). Based on point counting, the average measured quartz cement volume for the modelled Judy and Joanne channel sandstones is 2.2 and 5.2%, respectively (see the Supplementary material: Table S3). The concurrence between measured and modelled quartz cement volume for the Judy and Joanne channel sandstones was achieved at 98 and 97% clay-coat coverage, respectively (Fig. 16b, c). This implies that to limit the average quartz cement volume to the observed value of 2.2 and 5.2%, each detrital quartz grain must be 97–98% coated.

Chlorite coat coverage ranges from 78 to 98% in the Judy channel sandstones and from 15.9 to 69% in the Joanne channel sandstones (Table 5). In the Judy channel sandstones, the average chlorite coat coverage is 91% and this gives an average measured quartz cement volume of 2.2% (see Supplementary material: Table S3), which is lower than the modelled volume (9.1%, after 41 myr in the quartz cementation window), using a similar coating coverage of 91% (Fig. 16b). In the Joanne channel sandstones, the average chlorite coat coverage is 38% and this gives an average measured quartz cement volume of 5.2% (Supplementary material: Table S3), which is significantly lower than the modelled volume (25.9%, after 41 myr in the quartz cementation window) using a similar coating coverage of 38% (Fig. 16c). The lower measured quartz cement volume compared to the modelled volume in both sandstones can be attributed to the additional impacts of high pore fluid pressure and low vertical effective stress (VES), which inhibited mechanical compaction in the Skagerrak Formation sandstones (Nguyen *et al.* 2013; Grant *et al.* 2014; Stricker and Jones 2016; Stricker *et al.* 2016*a*). In general, chlorite clay coats have inhibited quartz cementation in the studied Skagerrak Formation sandstones; however, its effectiveness is dependent on its extent of coverage (or continuity) on the detrital grain surfaces.

Grain size and quartz cementation

In addition to clay coats, grain size has also been reported to have a significant effect on quartz cementation (Walderhaug 1996; Bloch *et al.* 2002). According to Walderhaug (1996), the surface area available for quartz cementation is a function of grain size. Finer grain sizes have a larger surface area than coarser grain sizes. As a result, finer-grained sandstones are likely to be more quartz cemented than coarser-grained sandstones (Walderhaug 1996; Bloch *et al.* 2002). In this study, however, very-fine-grained sandstones contain less quartz cement than fine- to medium-grained sandstones. This could be attributed to the higher clay-coat coverage in the very-fine-grained sandstones, which resulted in a significant reduction of available quartz-grain surface area for quartz precipitation. The quartz cementation model shows that prior to clay coating (0% coating coverage), the very-fine-grained Judy sandstones (average grain size 0.11 mm) have a higher quartz surface area (199 $cm^2\ cm^{-3}$) than the fine-grained Joanne sandstones (110.7 $cm^2\ cm^{-3}$) with an average grain size of 0.22 mm (Fig. 16d, e). Increasing the chlorite coat coverage to 91 and 38% (average measured values) in the Judy and Joanne channel sandstones, respectively, reduces the quartz surface area available for quartz precipitation to 17.9 $cm^2\ cm^{-3}$ in the Judy channel sandstones and 68.5 $cm^2\ cm^{-3}$ in the Joanne channel sandstones (Fig. 16d, e). This implies that finer-grained sandstones with extensive clay-coat coverage can become less quartz cemented than coarser-grained sandstones with a lesser clay-coat coverage. In general, the positive correlation between initial quartz surface area and quartz cement volume, as shown in Figure 16f, suggests that the available quartz surface area is a primary control on quartz cementation. In addition, clay coatings can inhibit quartz cementation by reducing the quartz surface area available for quartz precipitation (Walderhaug 1996, 2000).

Correlation between grain size and clay-coat coverage

In the studied datasets, a significant correlation exists between grain size and clay-coat coverage, with clay-coat coverage increasing with decreasing grain size (Figs 17a and 18). Average clay-coat coverage ranges from 78.5 to 98% in the finer-grained LEFC sandstones (average grain size <0.15 mm), whereas it ranges from 15.9 to 69% in their coarser-grained HEFC counterparts (average grain size >0.15 mm). This observation is consistent with those of previous studies, where clay-coat coverage has been reported to increase with decreasing grain size (Wilson 1992; Ajdukiewicz *et al.* 2010; Wooldridge *et al.* 2017). Furthermore, the lower clay-coat coverage characterizing the HEFC sandstones could be linked to the high degree of abrasion or reworking they were subjected to during sediment transport. During sediment transport, coarser grains experience a higher degree of abrasive transport than finer grains. As a result, clay coats can be more completely abraded on coarser grains than finer grains (Wilson 1992; Ajdukiewicz *et al.* 2010; Wooldridge *et al.* 2019*a*; Verhagen *et al.* 2020).

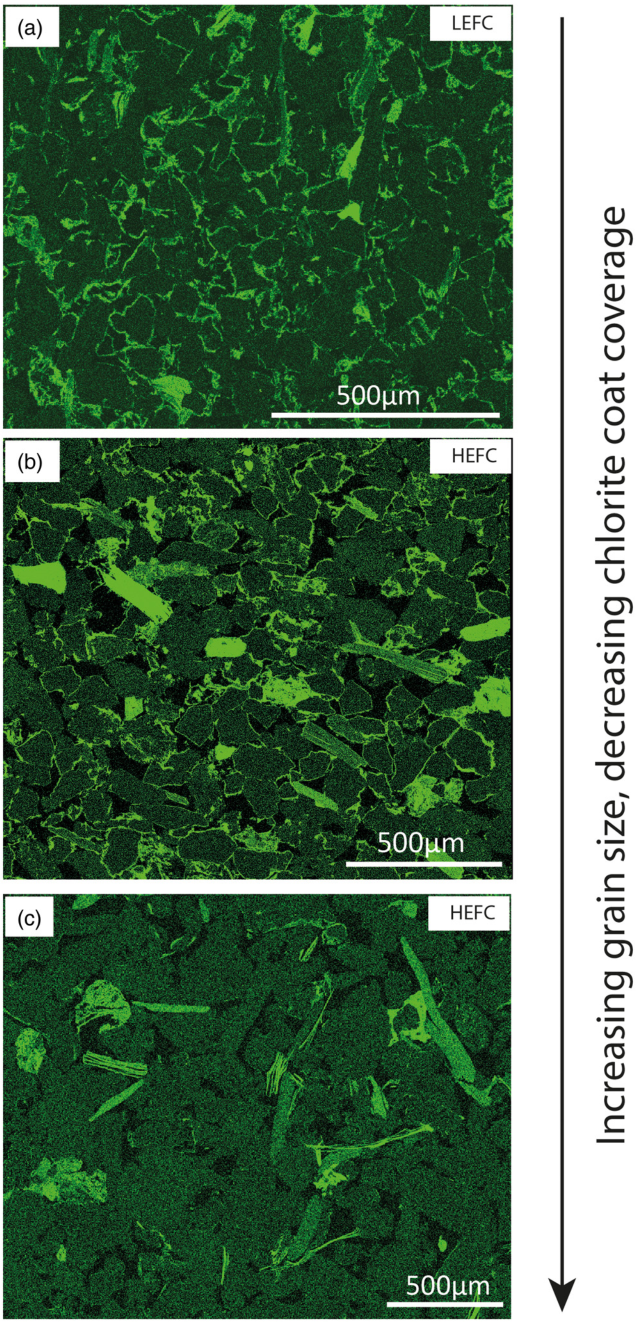

Fig. 18. Grain-coating phase maps of three representative chlorite-coated Skagerrak Formation sandstones showing the relationship between clay-coat coverage and grain size. (**a**) Low-energy fluvial channel (LEFC) sandstone: depth, 11 309.8 ft; average grain size, 93.3 µm (0.093 mm); average clay-coat coverage, 96%. (**b**) High-energy fluvial channel (HEFC) sandstone: depth: 11 496 ft; average grain size, 145 µm (0.145 mm); average clay-coat coverage, 80.4%. (**c**) High-energy fluvial channel (HEFC) sandstone: depth: 15 650.1 ft; average grain size, 216 µm (0.216 mm); average clay-coat coverage, 17%. Generally, the average clay-coat coverage reduces with increasing average grain size.

Correlation between clay volume and clay-coat coverage

Increased clay mineral volume (occurring mainly as coats) has been widely reported to enhance clay-coat coverage (Pittman *et al.* 1992; Wooldridge *et al.* 2019*b*; Charlaftis *et al.* 2022). In this study, a positive correlation exists between clay-coat coverage and clay-coat volume derived from point counting ($R = 0.77$) (Fig. 17b). Sandstones with >60% average clay-coat coverage contain clay-coat volumes in the range of 5–10%, while sandstones with ≤50% clay-coat coverage have <5% clay-coat volume (Fig. 17b; Table 5). With few exceptions, sandstones with >60% average clay-coat coverage and 5–10% clay-coat volume are restricted to the LEFC sandstone facies, while those with <50% clay-coat coverage and <5% clay-coat volume are restricted to the HEFC sandstone facies. This implies that variations in depositional energy exert a significant influence on the volume of detrital clay distributed as clay coats prior to final burial. This observation supports the assertion of Wooldridge *et al.* (2019*a*) that lower-energy environments generally have a greater volume of clay available for infiltration and higher degrees of clay-coat coverage than high-energy environments.

Microporosity and chlorite coats

Clay minerals in sandstones often contain considerable microporosity, which contributes to the total porosity from core analysis and wireline-log data (Hurst and Nadeau 1995). However, clay microporosity can introduce high irreducible water saturation, lowering the effective porosity and permeability (Hurst and Nadeau 1995; Xia *et al.* 2020). This study shows a positive correlation between microporosity and volume of chlorite coats, as well as a positive correlation between microporosity and chlorite coat coverage (Fig. 19a, b). Sandstones with >6% microporosity have a higher clay-coat volume (5–10%) and clay-coat coverage (60–98%). Conversely, those containing <6% microporosity have a lower clay-coat volume (1.3–5%) and clay-coat coverage (15.9–60%). In general, clay microporosity increases with increasing clay-coat volume and coverage.

Correlation between clay-coat coverage and porosity–permeability

Previous studies (Dutton *et al.* 2018; Bello *et al.* 2021) have established a positive correlation between clay-coat coverage and porosity–permeability. These studies showed that porosity and permeability increase with increasing clay coat coverage. However, in this study, such a positive correlation could not be established (Fig. 19c–e). In this study, sandstones with lower clay coat coverage (HEFC) have higher porosity (thin section) and permeability than those with higher clay coat coverage (LEFC). The porosity and permeability of the sandstones are primarily influenced by the depositional processes/energy of the system, which in turn control the distribution of grain size and clay content. The high porosity (thin section) and permeability exhibited by the HEFC sandstones, despite their low clay coat coverage and greater quartz cement volume, is due to their coarser grain sizes (fine–medium grained) and absence or minimal amounts of clays (Fig. 19f–i). In contrast, the low porosity (thin section) and permeability characterizing the LEFC sandstones, despite their higher clay coat coverage, is due to their finer grain sizes (very fine–fine grained) and the relatively higher amounts of clay (Fig. 19f–i). It is worth noting that the cross-plot of measured permeability and helium porosity for the selected sandstones in Figure 19j shows a poor correlation, in contrast to Figure 14a, b, which includes all of the investigated samples. This is due to the effect of clay microporosity on helium porosity. However, a strong positive correlation occurs when plotted with thin-section porosity (Fig. 19k).

Implications for reservoir quality prediction

It is a common practice to target clean (clay-free) sandstones and ignore their relatively clay-rich counterparts (Wooldridge *et al.* 2017). This is due to the general belief that the best reservoir quality occurs in clean and coarser-grained sandstones. As demonstrated in this study, cleaner and coarser-grained channel sandstones have better reservoir quality than finer-grained, clay-rich channel sandstones. However, the cleaner and coarser-grained channel

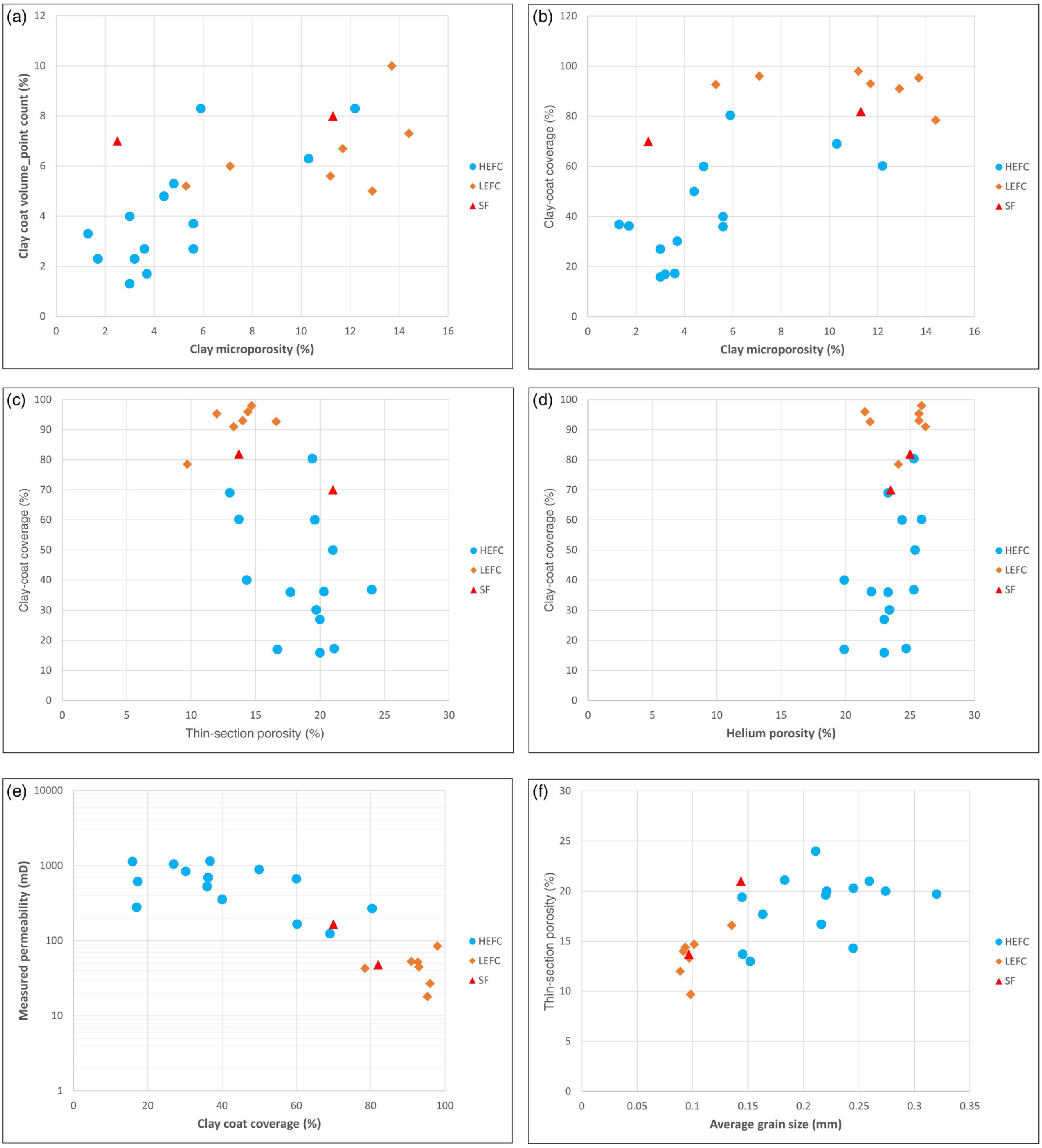

Fig. 19. Relationship between clay-coat volume, coverage and reservoir parameters for 23 of the studied sandstone samples from the Skagerrak Formation. (**a**) Cross-plot of clay-coat volume and microporosity. (**b**) Cross-plot of clay-coat coverage and microporosity. (**c**) and (**d**) Cross-plots of clay-coat coverage v. thin-section and helium porosity. (**e**) Cross-plot of measured permeability and clay-coat coverage. (**f**) and (**g**) Cross-plots of thin-section porosity and measured permeability v. grain size. (**h**) and (**i**) Cross-plots of thin-section porosity and permeability v. total clay. (**j**) Cross-plot of helium porosity and measured permeability (Note: unlike Fig. 14a, b, the plot does not show any clear correlation due to the effect of clay microporosity on helium porosity). (**k**) Plot of permeability against thin-section porosity showing a good correlation.

sandstones (HEFC) have a greater quartz cement volume due to a lesser clay coat coverage (<50%) on the detrital quartz-grain surfaces. Continuous burial of these clean, coarser-grained and less-coated sandstones into ultra-deep HPHT settings (>20 000 psi and >200°C) (Smithson 2016) could result in further quartz cementation and significant porosity–permeability loss. Conversely, the higher clay coat coverage (70–98%) in the finer-grained, slightly dirty channel sandstones (LEFC) will inhibit further quartz cementation, and help to preserve good porosity and moderate permeability, when buried in ultra-deep HPHT settings (Fig. 20).

It is also worth noting that increased clay content and clay-coat thickness in sandstones can have negative impacts on reservoir quality. Our study suggests that between 5 and 10% clay fraction (occurring primarily as clay coats) is required to form adequate clay coat coverage that can effectively inhibit quartz cementation and preserve favourable reservoir quality in deeply buried fluvial

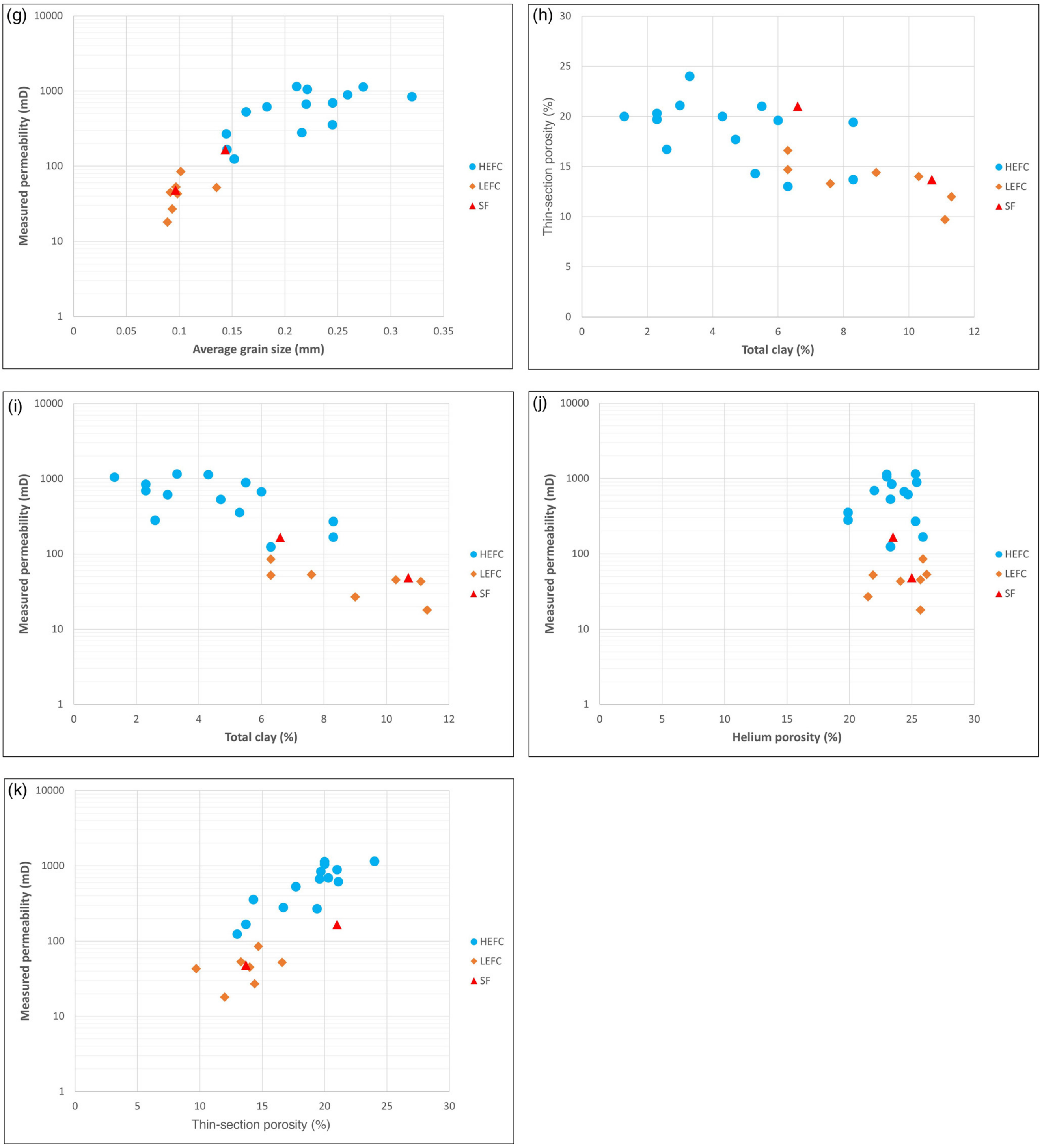

Fig. 19. Continued.

sandstones. This range is within the optimum range (5–13%) proposed by Pittman *et al.* (1992) for the Tuscaloosa Formation. Depending on pore-throat size, thicker clay coats can block pore throats and consequently inhibit fluid flow (Worden *et al.* 2020). Clay-coat thickness in this study ranges from 0.5 to 10 µm (except in embayed surfaces where it is up to 16 µm) and has not resulted in the blockage of pore throats. These thickness values are within the 5–10 µm range reported as beneficial for reservoir quality preservation (Anjos *et al.* 2003; Sun *et al.* 2014; Charlaftis *et al.* 2021).

The impacts of authigenic chlorite on wireline logs (particularly neutron and resistivity logs) have been highlighted in the literature (Nadeau 2000; Bloch *et al.* 2002; Worden *et al.* 2020; Azzam *et al.* 2022). Chlorite contains more hydrogen atoms than illite, and therefore gives rise to high neutron responses and, ultimately, additional porosity. The presence of microporous grain-coating or pore-filling chlorite in sandstones commonly results in anomalously high water saturation. Consequently, low resistivity can result even in oil-bearing sandstones (Anjos *et al.* 1999; Xia *et al.* 2020). Ultimately, this can lead to underestimating the recoverable hydrocarbon resources during field appraisal and development. This implies that low reservoir quality intervals (dirty sandstones), previously regarded as non-productive zones in ageing and matured fields, need to be carefully re-evaluated. This can help to replenish reserves and increase production/recovery.

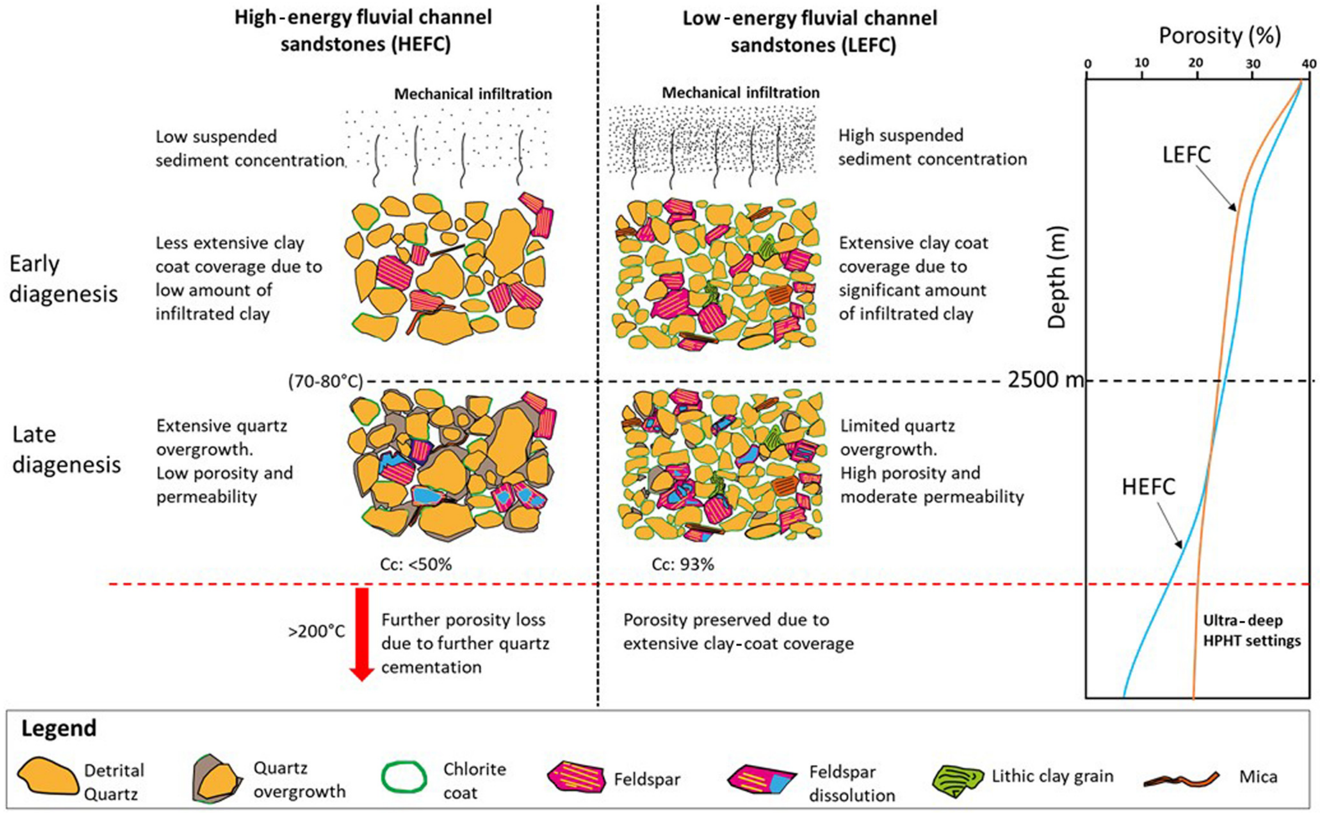

Fig. 20. Schematic illustration of diagenetic and related reservoir quality evolution pathways in high- and low-energy fluvial channel sandstone reservoirs (Cc, average clay-coat coverage).

Conclusions

(1) The reservoir quality (porosity and permeability) of the deeply buried HPHT Triassic Skagerrak fluvial sandstones is primarily controlled by depositional facies/processes, grain size and clay content.

(2) The confined fluvial channel facies constitute the best reservoirs, while the floodplain, palaeosols and lake facies form poor to non-reservoirs. However, within the channel facies, there is a variation in reservoir quality. The high-energy channel sandstones have higher reservoir quality (100–1150 mD) due to their coarser grain size and lower clay content. The low-energy channel sandstones, on the other hand, have lower reservoir quality (<100 mD) due to their finer grain size and slightly higher clay content.

(3) Petrographic and SEM analysis revealed that the preservation of good reservoir quality in these channel sandstones is also partly due to the presence of grain-coating chlorite that inhibited the extensive growth of quartz cement.

(4) In this study, clay coat coverage (the principal factor controlling the ability of grain-coating clays to effectively inhibit quartz cementation) can be linked to depositional facies, grain size, clay-coat volume and depositional energy. Higher clay coat coverage (70–98%) occurs in finer-grained, low-energy channel sandstones containing between 5 and 10% clay-coat volume, while lesser clay coat coverage (<50%) is found in coarser-grained, high-energy channel sandstones containing <5% clay-coat volume.

(5) Clean sands have been highlighted as being the best starting material for good reservoir quality at depth. This study demonstrates that clay-rich fluvial channel and crevasse splay sandstones with moderate amounts of clay, mostly in the form of clay coats, could equally offer good reservoir quality.

Acknowledgements We acknowledge support from the BGS in providing access to core materials from the Jade and Judy wells. We would also like to thank Ian Chaplin and Sophie Edwards for thin-section preparations, and Leon Bowen and Alvarez-Ruiz Diana for providing support during the SEM analysis. We would like to thank the reviewers for their careful consideration of our manuscript.

Author contributions **OEA**: conceptualization (lead), data curation (lead), formal analysis (equal), funding acquisition (lead), investigation (lead), methodology (equal), software (lead), visualization (equal), writing – original draft (lead), writing – review & editing (equal); **SJJ**: conceptualization (supporting), formal analysis (equal), methodology (equal), supervision (lead), visualization (equal), writing – review & editing (supporting); **NSM**: conceptualization (supporting), formal analysis (equal), methodology (equal), supervision (supporting), writing – review & editing (supporting); **JG**: supervision (supporting), visualization (equal), writing – review & editing (supporting); **DC**: visualization (equal), writing – review & editing (supporting).

Funding This work was funded by the Petroleum Technology Development Fund (grant No. PTDF/ED/PHD/AOE/1168/17 awarded to O.E. Aro).

Competing interests The authors declare that they have no known competing financial interests or personal relationships that could have appeared to influence the work reported in this paper.

Data availability All data generated or analysed during this study are included in this published article (and its supplementary information files).

References

Ajdukiewicz, J.M. and Lander, R.H. 2010. Sandstone reservoir quality prediction: the state of the art. *AAPG Bulletin*, **94**, 1083–1091, https://doi.org/10.1306/intro060110

Ajdukiewicz, J.M. and Larese, R.E. 2012. How clay grain coats inhibit quartz cement and preserve porosity in deeply buried sandstones: observations and experiments. *AAPG Bulletin*, **96**, 2091–2119, https://doi.org/10.1306/02211211075

Ajdukiewicz, J.M., Nicholson, P.H. and Esch, W.L. 2010. Prediction of deep reservoir quality using early diagenetic process models in the Jurassic Norphlet Formation, Gulf of Mexico. *AAPG Bulletin*, **94**, 1189–1227, https://doi.org/10.1306/04211009152

Akpokodje, M., Melvin, A. *et al.* 2017. Regional study of controls on reservoir quality in the Triassic Skagerrak Formation of the Central North Sea. *Geological Society, London, Petroleum Geology Conference Series*, **8**, 125–146, https://doi.org/10.1144/PGC8.29

Allen, P.A. and Allen, J.R. 2005. *Basin Analysis: Principles and Applications*. 2nd edn. Blackwell, Oxford, UK.

Andrews-Speed, C.P., Oxburgh, E.R. and Cooper, B.A. 1984. Temperatures and depth-dependent heat flow in western North Sea. *AAPG Bulletin*, **68**, 1764–1781, https://doi.org/10.1306/AD461999-16F7-11D7-8645000102C1865D

Anjos, S.M.C., De Ros, L.F. and Silva, C.M.A. 2003. Chlorite authigenesis and porosity preservation in the Upper Cretaceous marine sandstones of the Santos Basin, offshore eastern Brazil. *In:* Worden, R.H., Morad, S. (Eds) *Clay Cements in Sandstones*. Special Publication of the International Association of Sedimentologists. Blackwells, Oxford, 291–316.

Azzam, F., Blaise, T. *et al.* 2022. Diagenesis and reservoir quality evolution of the Lower Cretaceous turbidite sandstones of the Agat Formation (Norwegian North Sea): Impact of clay grain coating and carbonate cement. *Marine and Petroleum Geology*, **142**, 105768, https://doi.org/10.1016/j.marpetgeo.2022.105768

Bahlis, A.B. and De Ros, L.F. 2013. Origin and impact of authigenic chlorite in the Upper Cretaceous sandstone reservoirs of the Santos Basin, eastern Brazil. *Petroleum Geoscience*, **19**, 185–199, https://doi.org/10.1144/petgeo2011-007

Baker, J.C. 1991. Diagenesis and reservoir quality of the Aldebaran Sandstone, Denison Trough, east-central Queensland, Australia. *Sedimentology*, **38**, 819–838, https://doi.org/10.1111/j.1365-3091.1991.tb01874.x

Barshep, D.V. and Worden, R.H. 2021. Reservoir quality of Upper Jurassic Corallian Sandstones, Weald Basin, UK. *Geosciences*, **11**, 446, https://doi.org/10.3390/geosciences11110446

Bello, A.M., Jones, S., Gluyas, J., Acikalin, S. and Cartigny, M. 2021. Role played by clay content in controlling reservoir quality of submarine fan system, Forties Sandstone Member, Central Graben, North Sea. *Marine and Petroleum Geology*, **128**, 105058, https://doi.org/10.1016/j.marpetgeo.2021.105058

Billault, V., Beaufort, D., Baronnet, A. and Lacharpagne, J.-C. 2003. A nanopetrographic and textural study of grain-coating chlorites in sandstone reservoirs. *Clay Minerals*, **38**, 315–328, https://doi.org/10.1180/0009855033830098

Bjørlykke, K. 2014. Relationships between depositional environments, burial history and rock properties. Some principal aspects of diagenetic process in sedimentary basins. *Sedimentary Geology*, **301**, 1–14, https://doi.org/10.1016/j.sedgeo.2013.12.002

Bjørlykke, K. and Egeberg, P. 1993. Quartz cementation in sedimentary basins. *AAPG Bulletin*, **77**, 1538–1548, https://doi.org/10.1306/BDFF8EE8-1718-11D7-8645000102C1865D

Bloch, S., Lander, R.H. and Bonnell, L. 2002. Anomalously high porosity and permeability in deeply buried sandstone reservoirs: origin and predictability. *AAPG Bulletin*, **86**, 301–328, https://doi.org/10.1306/61EEDABC-173E-11D7-8645000102C1865D

Bridge, J.S. and Lunt, I.A. 2006. Depostional models of braided rivers. *International Association of Sedimentologists Special Publications*, **36**, 11–50, https://doi.org/10.1002/9781444304374.ch2

Bridge, J.S., Alexander, J., Collier, R.E.L., Gawthorpe, R.L. and Jarvis, J. 1995. Ground-penetrating radar and coring used to study the large-scale structure of point-bar deposits in three dimensions. *Sedimentology*, **42**, 839–852, https://doi.org/10.1111/j.1365-3091.1995.tb00413.x

Brown, S. 1991. Stratigraphy of the oil and gas reservoirs: UK Continental Shelf. *Geological Society, London, Memoirs*, **14**, 9–18, https://doi.org/10.1144/GSL.MEM.1991.014.01.02

Bukar, M., Worden, R.H., Bukar, S. and Shell, P. 2021. Diagenesis and its controls on reservoir quality of the Tambar oil field, Norwegian North Sea. *Energy Geoscience*, **2**, 10–31, https://doi.org/10.1016/j.engeos.2020.07.002

Burgess, R., Jolley, D. and Hartley, A. 2020. Stratigraphic palynology of the Middle–Late Triassic successions of the Central North Sea. *Petroleum Geoscience*, **27**, https://doi.org/10.1144/petgeo2019-128

Cameron, T.D.J. 1993. 4. Triassic, Permian and pre-Permian of the central and northern North Sea. *In:* Knox, R.W.O'B. and Cordey, W.G. (eds) *Lithostratigraphic Nomenclature of the UK North Sea*. British Geological Survey, Keyworth, Nottingham, UK.

Charlaftis, D., Jones, S.J., Dobson, K.J., Crouch, J. and Acikalin, S. 2021. Experimental study of chlorite authigenesis and influence on porosity maintenance in sandstones. *Journal of Sedimentary Research*, **91**, 197–212, https://doi.org/10.2110/jsr.2020.122

Charlaftis, D., Dobson, K., Jones, S.J., Lakshtanov, D., Crouch, J. and Cook, J. 2022. Experimental simulation of burial diagenesis and subsequent 2D–3D characterization of sandstone reservoir quality. *Frontiers in Earth Science*, **10**, https://doi.org/10.3389/feart.2022.766145

di Primio, R. and Neumann, V. 2008. HPHT reservoir evolution: a case study from Jade and Judy fields, Central Graben, UK North Sea. *International Journal of Earth Sciences*, **97**, 1101–1114, https://doi.org/10.1007/s00531-007-0206-y

Dowey, P.J., Hodgson, D.M. and Worden, R.H. 2012. Pre-requisites, processes, and prediction of chlorite grain coatings in petroleum reservoirs: A review of subsurface examples. *Marine and Petroleum Geology*, **32**, 63–75, https://doi.org/10.1016/j.marpetgeo.2011.11.007

Dowey, P.J., Worden, R.H., Utley, J. and Hodgson, D.M. 2017. Sedimentary controls on modern sand grain coat formation. *Sedimentary Geology*, **353**, 46–63, https://doi.org/10.1016/j.sedgeo.2017.03.001

Dutton, S.P., Hutton, M.E., Ambrose, W.A., Childers, A.T. and Loucks, R.G. 2018. Preservation of reservoir quality by chlorite coats in deep Tuscaloosa sandstones, Central Louisiana, USA. *Gulf Coast Association of Geological Societies*, **7**, 46–58.

Ehrenberg, S.N. 1990. Relationship between diagenesis and reservoir quality in sandstones of the Garn Formation, Haltenbanken, mid-Norwegian continental shelf. *AAPG Bulletin*, **74**, 1538–1558, https://doi.org/10.1306/0C9B2515-1710-11D7-8645000102C1865D

Ehrenberg, S.N. 1993. Preservation of anomalously high porosity in deeply buried sandstones by grain-coating chlorite: examples from the Norwegian continental shelf. *AAPG Bulletin*, **77**, 1260–1286, https://doi.org/10.1306/BDFF8E5C-1718-11D7-8645000102C1865D

Folk, R.L. 1980. *Petrology of Sedimentary Rocks*. Hemphill Publishing, Houston, TX.

Folk, R.L. and Ward, W.C. 1957. Brazos River bar [Texas]; a study in the significance of grain size parameters. *Journal of Sedimentary Research*, **27**, 3–26, https://doi.org/10.1306/74D70646-2B21-11D7-8648000102C1865D

Gier, S., Worden, R.H., Johns, W.D. and Kurzweil, H. 2008. Diagenesis and reservoir quality of Miocene sandstones in the Vienna Basin, Austria. *Marine and Petroleum Geology*, **25**, 681–695, https://doi.org/10.1016/j.marpetgeo.2008.06.001

Glennie, K.W. 1998. *Petroleum Geology of the North Sea: Basic Concepts and Recent Advances*. 4th edn. Blackwell Science, Oxford, UK.

Gluyas, J. and Cade, C.A. 1997. Prediction of porosity in compacted sands. *AAPG Memoirs*, **69**, 19–28.

Goldsmith, P.J., Rich, B. and Standring, J. 1995. Triassic correlation and stratigraphy in the South Central Graben, UK North Sea. *Geological Society, London, Special Publications*, **91**, 123–143, https://doi.org/10.1144/GSL.SP.1995.091.01.07

Goldsmith, P.J., Hudson, G. and Van Veen, P. 2003. Triassic. *In:*Evans, D., Graham, C., Armour, A. and Bathurst, P. (eds) *The Millennium Atlas: Petroleum Geology of the Central and Northern North Sea*. Geological Society, London, 105–127.

Gowers, M.B. and Sæbøe, A. 1985. On the structural evolution of the Central Trough in the Norwegian and Danish sectors of the North Sea. *Marine and Petroleum Geology*, **2**, 298–318, https://doi.org/10.1016/0264-8172(85)90026-1

Gradstein, F.M., Agterberg, F.P., Ogg, J.G., Hardenbol, J., Van Veen, P., Thierry, J. and Huang, Z. 1995. A Triassic, Jurassic and Cretaceous time scale. *SEPM Special Publications*, **54**, 95–126, https://doi.org/10.2110/pec.95.04.0095

Grant, N.T., Middleton, A.J. and Archer, S. 2014. Porosity trends in the Skagerrak Formation, Central Graben, United Kingdom Continental Shelf: the role of compaction and pore pressure history. *AAPG Bulletin*, **98**, 1111–1143, https://doi.org/10.1306/10211313002

Gray, E., Hartley, A. and Howell, J. 2020. The influence of stratigraphy and facies distribution on reservoir quality and production performance in the Triassic Skagerrak Formation of the UK and Norwegian Central North Sea. *Geological Society, London, Special Publications*, **494**, 379–409, https://doi.org/10.1144/sp494-2019-68

Heald, M. and Larese, R. 1974. Influence of coatings on quartz cementation. *Journal of Sedimentary Research*, **44**, 1269–1274.

Hodgson, N.A., Farnsworth, J. and Fraser, A.J. 1992. Salt-related tectonics, sedimentation and hydrocarbon plays in the Central Graben, North Sea, UKCS. *Geological Society, London, Special Publications*, **67**, 31–63, https://doi.org/10.1144/GSL.SP.1992.067.01.03

Houseknecht, D.W. 1987. Assessing the relative importance of compaction processes and cementation to reduction of porosity in sandstones. *AAPG Bulletin*, **71**, 633–642, https://doi.org/10.1306/9488787F-1704-11D7-8645000102C1865D

Houseknecht, D.W. 1988. Intergranular pressure solution in four quartzose sandstones. *Journal of Sedimentary Research*, **58**, 228–246, https://doi.org/10.1306/212F8D64-2B24-11D7-8648000102C1865D

Humphreys, B., Smith, S.A. and Strong, G.E. 1989. Authigenic chlorite in late Triassic sandstones from the Central Graben, North Sea. *Clay Minerals*, **24**, 427–444, https://doi.org/10.1180/claymin.1989.024.2.17

Humphreys, B., Kemp, S., Lott, G., Dharmayanti, D. and Samsori, I. 1994. Origin of grain-coating chlorite by smectite transformation: an example from Miocene sandstones, North Sumatra back-arc basin, Indonesia. *Clay Minerals*, **29**, 681–692, https://doi.org/10.1180/claymin.1994.029.4.21

Hurst, A. and Nadeau, P.H. 1995. Clay microporosity in reservoir sandstones: an application of quantitative electron microscopy in petrophysical evaluation. *AAPG Bulletin*, **79**, 563–573, https://doi.org/10.1306/8D2B1598-171E-11D7-8645000102C1865D

Isaksen, G.H. 2004. Central North Sea hydrocarbon systems: generation, migration, entrapment, and thermal degradation of oil and gas. *AAPG Bulletin*, **88**, 1545–1572, https://doi.org/10.1306/06300403048

Johnson, H. and Lott, G.K. 1993. 2. Cretaceous of the Central and Northern North Sea. *In*: Knox, R.W.O'B. and Cordey, W.G. (eds) *Lithostratigraphic Nomenclature of the UK North Sea*. British Geological Survey, Keyworth, Nottingham, UK.

Jones, A.D., Auld, H.A., Carpenter, T.J., Fetkovich, E., Palmer, I.A., Rigatos, E.N. and Thompson, M.W. 2005. Jade Field: an innovative approach to high-pressure, high-temperature field development. *Geological Society, London, Petroleum Geology Conference Series*, **6**, 269–283, https://doi.org/10.1144/0060269

Keller, T., Bayes, R., Auld, H. and Lines, M. 2005. Judy Field: rejuvenation through a second phase of drilling. *In:* Doré, A.G. and Vining, B.A. (eds) *Geological Society, London, Petroleum Geology Conference Series*, **6**, 651–661, https://doi.org/10.1144/0060651

Knox, R.W.O'B. and Holloway, S. 1992. 1. Paleogene of the Central and Northern North Sea. *In:* Knox, R.W.O'B. and Cordey, W.G. (eds) *Lithostratigraphic Nomenclature of the UK North Sea*. British Geological Survey, Keyworth, Nottingham, UK.

Kozeny, J. 1927. Uber kapillare Leitung der Wassers im Boden. *Royal Academy of Science, Vienna, Proceedings, Class I*, **136**, 271–306.

Lai, J., Wang, G. *et al.* 2018. A review on pore structure characterization in tight sandstones. *Earth-Science Reviews*, **177**, 436–457, https://doi.org/10.1016/j.earscirev.2017.12.003

Lala, A.M.S. and El-Sayed, N.A. 2017. Controls of pore throat radius distribution on permeability. *Journal of Petroleum Science and Engineering*, **157**, 941–950, https://doi.org/10.1016/j.petrol.2017.08.005

Lander, R.H., Larese, R.E. and Bonnell, L.M. 2008. Toward more accurate quartz cement models: the importance of euhedral versus noneuhedral growth rates. *AAPG Bulletin*, **92**, 1537–1563, https://doi.org/10.1306/07160808037

Leeder, M. 1973. Fluviatile fining-upwards cycles and the magnitude of palaeochannels. *Geological Magazine*, **110**, 265–276, https://doi.org/10.1017/S0016756800036098

Lundegard, P.D. 1992. Sandstone porosity loss; a 'big picture' view of the importance of compaction. *Journal of Sedimentary Research*, **62**, 250–260, https://doi.org/10.1306/D42678D4-2B26-11D7-8648000102C1865D

Mahmic, O., Dypvik, H. and Hammer, E. 2018. Diagenetic influence on reservoir quality evolution, examples from Triassic conglomerates/arenites in the Edvard Grieg field, Norwegian North Sea. *Marine and Petroleum Geology*, **93**, 247–271, https://doi.org/10.1016/j.marpetgeo.2018.03.006

Matlack, K.S., Houseknecht, D.W. and Applin, K.R. 1989. Emplacement of clay into sand by infiltration. *Journal of Sedimentary Research*, **59**, 77–87, https://doi.org/10.1306/212F8F21-2B24-11D7-8648000102C1865D

McBride, E.F. 1989. Quartz cement in sandstones: a review. *Earth-Science Reviews*, **26**, 69–112, https://doi.org/10.1016/0012-8252(89)90019-6

McKie, T. 2011. Architecture and behavior of dryland fluvial reservoirs, Triassic Skagerrak Formation, central North Sea. *SEPM Special Publications*, **97**, 189–214, https://doi.org/10.2110/sepmsp.097.189

McKie, T. 2014. Climatic and tectonic controls on Triassic dryland terminal fluvial system architecture, central North Sea. *International Association of Sedimentologists Special Publications*, **46**, 19–58, https://doi.org/10.1002/9781118920435.ch2

McKie, T. and Audretsch, P. 2005. Depositional and structural controls on Triassic reservoir performance in the Heron Cluster, ETAP, Central North Sea. *Geological Society, London, Petroleum Geology Conference Series*, **6**, 285–297, https://doi.org/10.1144/0060285

McKie, T., Jolley, S.J. and Kristensen, M.B. 2010. Stratigraphic and structural compartmentalization of dryland fluvial reservoirs: Triassic Heron Cluster, Central North Sea. *Geological Society, London, Special Publications*, **347**, 165–198, https://doi.org/10.1144/SP347.11

McKinley, J.M., Worden, R.H. and Ruffell, A.H. 2003. Smectite in sandstones: A review of the controls on occurrence and behaviour during diagenesis. *International Association of Sedimentologists Special Publications*, **34**, 109–128, https://doi.org/10.1002/9781444304336.ch5

Molenaar, N., Cyziene, J. and Sliaupa, S. 2007. Quartz cementation mechanisms and porosity variation in Baltic Cambrian sandstones. *Sedimentary Geology*, **195**, 135–159, https://doi.org/10.1016/j.sedgeo.2006.07.009

Morad, S., Ketzer, J. and De Ros, L.F. 2000. Spatial and temporal distribution of diagenetic alterations in siliciclastic rocks: implications for mass transfer in sedimentary basins. *Sedimentology*, **47**, 95–120, https://doi.org/10.1046/j.1365-3091.2000.00007.x

Morad, S., Al-Ramadan, K., Ketzer, J.M. and De Ros, L.F. 2010. The impact of diagenesis on the heterogeneity of sandstone reservoirs: a review of the role of depositional facies and sequence stratigraphy. *AAPG Bulletin*, **94**, 1267–1309, https://doi.org/10.1306/04211009178

Moraes, M.A. and De Ros, L.F. 1992. Depositional, infiltrated and authigenic clays in fluvial sandstones of the Jurassic Sergi Formation, Recôncavo Basin, northeastern Brazil. *SEPM Special Publications*, **47**, 197–208, https://doi.org/10.2110/pec.92.47.0197

Mouritzen, C., Farris, M.A., Morton, A. and Matthews, S. 2017. Integrated Triassic stratigraphy of the greater Culzean area, UK central North Sea. *Petroleum Geoscience*, **24**, 197–207, https://doi.org/10.1144/petgeo2017-039

Nadeau, P.H. 2000. The Sleipner Effect: A subtle relationship between the distribution of diagenetic clay, reservoir porosity, permeability, and water saturation. *Clay Minerals*, **35**, 185–200, https://doi.org/10.1180/000985500546576

Nelson, P.H. 2009. Pore-throat sizes in sandstones, tight sandstones, and shales. *AAPG Bulletin*, **93**, 329–340, https://doi.org/10.1306/10240808059

Nguyen, B.T., Jones, S.J., Goulty, N.R., Middleton, A.J., Grant, N., Ferguson, A. and Bowen, L. 2013. The role of fluid pressure and diagenetic cements for porosity preservation in Triassic fluvial reservoirs of the Central Graben, North Sea. *AAPG Bulletin*, **97**, 1273–1302, https://doi.org/10.1306/01151311163

Nichols, G. and Fisher, J. 2007. Processes, facies and architecture of fluvial distributary system deposits. *Sedimentary Geology*, **195**, 75–90, https://doi.org/10.1016/j.sedgeo.2006.07.004

Olivarius, M., Weibel, R., Hjuler, M.L., Kristensen, L., Mathiesen, A., Nielsen, L.H. and Kjøller, C. 2015. Diagenetic effects on porosity–permeability relationships in red beds of the Lower Triassic Bunter Sandstone Formation in the North German Basin. *Sedimentary Geology*, **321**, 139–153, https://doi.org/10.1016/j.sedgeo.2015.03.003

Oluwadebi, A.G., Taylor, K.G. and Dowey, P.J. 2018. Diagenetic controls on the reservoir quality of the tight gas Collyhurst Sandstone Formation, Lower Permian, East Irish Sea Basin, United Kingdom. *Sedimentary Geology*, **371**, 55–74, https://doi.org/10.1016/j.sedgeo.2018.04.006

Osborne, M.J. and Swarbrick, R.E. 1997. Mechanisms for generating overpressure in sedimentary basins: a reevaluation. *AAPG Bulletin*, **81**, 1023–1041, https://doi.org/10.1306/522B49C9-1727-11D7-8645000102C1865D

Oye, O.J., Aplin, A.C., Jones, S.J., Gluyas, J.G., Bowen, L., Orland, I.J. and Valley, J.W. 2018. Vertical effective stress as a control on quartz cementation in sandstones. *Marine and Petroleum Geology*, **98**, 640–652, https://doi.org/10.1016/j.marpetgeo.2018.09.017

Paxton, S., Szabo, J., Ajdukiewicz, J. and Klimentidis, R. 2002. Construction of an intergranular volume compaction curve for evaluating and predicting compaction and porosity loss in rigid-grain sandstone reservoirs. *AAPG Bulletin*, **86**, 2047–2067, https://doi.org/10.1306/61EEDDFA-173E-11D7-8645000102C1865D

Pittman, E.D., Larese, R.E. and Heald, M.T. 1992. Clay coats: occurrence and relevance to preservation of porosity in sandstones. *SEPM Special Publications*, **47**, 241–264, https://doi.org/10.2110/pec.92.47.0241

Richards, P.C., Lott, G.K., Johnson, H., Knox, R.W.O. and Riding, J.B. 1993. 3. Jurassic of the Central and Northern North Sea. *In:* Knox, R.W.O'B. and Cordey, W.G. (eds) *Lithostratigraphic Nomenclature of the UK North Sea*. British Geological Survey, Keyworth, Nottingham, UK.

Schmid, S., Worden, R.H. and Fisher, Q.J. 2004. Diagenesis and reservoir quality of the Sherwood Sandstone (Triassic), Corrib Field, Slyne Basin, west of Ireland. *Marine and Petroleum Geology*, **21**, 299–315, https://doi.org/10.1016/j.marpetgeo.2003.11.015

Shelukhina, O., El-Ghali, M.A. *et al.* 2021. Origin and control of grain-coating clays on the development of quartz overgrowths: example from the lower Paleozoic Barik Formation sandstones, Huqf region, Oman. *Arabian Journal of Geosciences*, **14**, 210, https://doi.org/10.1007/s12517-021-06541-5

Smith, R.I., Hodgson, N. and Fulton, M. 1993. Salt control on Triassic reservoir distribution, UKCS Central North Sea. *Geological Society, London, Petroleum Geology Conference Series*, **4**, 547–557, https://doi.org/10.1144/0040547

Smithson, T. 2016. HPHT wells. *Oilfield Review*, **2016**, https://www.slb.com/-/media/files/oilfield-review/defining-hpht.ashx

Steel, R. and Ryseth, A. 1990. The Triassic–early Jurassic succession in the northern North Sea: megasequence stratigraphy and intra-Triassic tectonics. *Geological Society, London, Special Publications*, **55**, 139–168, https://doi.org/10.1144/GSL.SP.1990.055.01.07

Storvoll, V., Bjørlykke, K., Karlsen, D. and Saigal, G. 2002. Porosity preservation in reservoir sandstones due to grain-coating illite: a study of the Jurassic Garn Formation from the Kristin and Lavrans fields, offshore Mid-Norway. *Marine and Petroleum Geology*, **19**, 767–781, https://doi.org/10.1016/S0264-8172(02)00035-1

Stricker, S. and Jones, S.J. 2016. Enhanced porosity preservation by pore fluid overpressure and chlorite grain coatings in the Triassic Skagerrak, Central Graben, North Sea, UK. *Geological Society, London, Special Publications*, **435**, 321–341, https://doi.org/10.1144/SP435.4

Stricker, S., Jones, S.J. and Grant, N.T. 2016*a*. Importance of vertical effective stress for reservoir quality in the Skagerrak Formation, Central Graben, North Sea. *Marine and Petroleum Geology*, **78**, 895–909, https://doi.org/10.1016/j.marpetgeo.2016.03.001

Stricker, S., Jones, S.J., Sathar, S., Bowen, L. and Oxtoby, N. 2016*b*. Exceptional reservoir quality in HPHT reservoir settings: Examples from the Skagerrak Formation of the Heron Cluster, North Sea, UK. *Marine and Petroleum Geology*, **77**, 198–215, https://doi.org/10.1016/j.marpetgeo.2016.02.003

Stricker, S., Jones, S.J., Meadows, N. and Bowen, L. 2018. Reservoir quality of fluvial sandstone reservoirs in salt-walled mini-basins: an example from the Seagull field, Central Graben, North Sea, UK. *Petroleum Science*, **15**, 1–27, https://doi.org/10.1007/s12182-017-0206-x

Sun, Z.-X., Sun, Z.-L., Yao, J., Wu, M.-L., Liu, J.-R., Dou, Z. and Pei, C. 2014. Porosity preservation due to authigenic chlorite coatings in deeply buried Upper Triassic Xujiahe Formation sandstones, Sichuan Basin, western China. *Journal of Petroleum Geology*, **37**, 251–267, https://doi.org/10.1111/jpg.12582

Swarbrick, R.E., Osborne, M.J. *et al.* 2000. Integrated study of the Judy Field (Block 30/7a) – an overpressured Central North Sea oil/gas field. *Marine and Petroleum Geology*, **17**, 993–1010, https://doi.org/10.1016/S0264-8172(00)00050-7

Tang, L.-x, Gluyas, J. and Jones, S. 2018*a*. Porosity preservation due to grain coating illite/smectite: Evidence from Buchan Formation (Upper Devonian) of the Ardmore Field, UK North Sea. *Proceedings of the Geologists' Association*, **129**, 202–214, https://doi.org/10.1016/j.pgeola.2018.03.001

Tang, L.-X., Gluyas, J., Jones, S. and Bowen, L. 2018*b*. Diagenetic and geochemical studies of the Buchan Formation (Upper Devonian) in the Central North Sea. *Petroleum Science*, **15**, 211–229, https://doi.org/10.1007/s12182-018-0232-3

Taylor, T.R., Giles, M.R. *et al.* 2010. Sandstone diagenesis and reservoir quality prediction: models, myths, and reality. *AAPG Bulletin*, **94**, 1093–1132, https://doi.org/10.1306/04211009123

Taylor, T.R., Kittridge, M.G., Winefield, P., Bryndzia, L.T. and Bonnell, L.M. 2015. Reservoir quality and rock properties modeling – Triassic and Jurassic sandstones, greater Shearwater area, UK Central North Sea. *Marine and Petroleum Geology*, **65**, 1–21, https://doi.org/10.1016/j.marpetgeo.2015.03.020

Verhagen, I.T.E., Crisóstomo-Figueroa, A., Utley, J.E.P. and Worden, R.H. 2020. Abrasion of detrital grain-coating clays during sediment transport: implications for diagenetic clay coats. *Sedimentary Geology*, **403**, 105653, https://doi.org/10.1016/j.sedgeo.2020.105653

Virolle, M., Brigaud, B. *et al.* 2019. Influence of sedimentation and detrital clay grain coats on chloritized sandstone reservoir qualities: Insights from comparisons between ancient tidal heterolithic sandstones and a modern estuarine system. *Marine and Petroleum Geology*, **107**, 163–184, https://doi.org/10.1016/j.marpetgeo.2019.05.010

Walderhaug, O. 1994*a*. Temperatures of quartz cementation in Jurassic sandstones from the Norwegian continental shelf; evidence from fluid inclusions. *Journal of Sedimentary Research*, **64**, 311–323, https://doi.org/10.1306/D4267D89-2B26-11D7-8648000102C1865D

Walderhaug, O. 1994*b*. Precipitation rates for quartz cement in sandstones determined by fluid-inclusion microthermometry and temperature–history modeling. *Journal of Sedimentary Research*, **64**, 324–333, https://doi.org/10.2110/jsr.64.324

Walderhaug, O. 1996. Kinetic modeling of quartz cementation and porosity loss in deeply buried sandstone reservoirs. *AAPG Bulletin*, **80**, 731–745, https://doi.org/10.1306/64ED88A4-1724-11D7-8645000102C1865D

Walderhaug, O. 2000. Modeling quartz cementation and porosity in Middle Jurassic Brent Group sandstones of the Kvitebjørn field, northern North Sea. *AAPG Bulletin*, **84**, 1325–1339, https://doi.org/10.1306/A9673E96-1738-11D7-8645000102C1865D

Walderhaug, O., Eliassen, A. and Aase, N.E. 2012. Prediction of permeability in quartz-rich sandstones: examples from the Norwegian continental shelf and the Fontainebleau sandstone. *Journal of Sedimentary Research*, **82**, 899–912, https://doi.org/10.2110/jsr.2012.79

Wilson, M.D. 1992. Inherited grain-rimming clays in sandstones from eolian and shelf environments: Their origin and control on reservoir properties. *SEPM Special Publications*, **47**, 209–225, https://doi.org/10.2110/pec.92.47.0209

Wolela, A.M. and Gierlowski-Kordesch, E.H. 2007. Diagenetic history of fluvial and lacustrine sandstones of the Hartford Basin (Triassic–Jurassic), Newark Supergroup, USA. *Sedimentary Geology*, **197**, 99–126, https://doi.org/10.1016/j.sedgeo.2006.09.006

Wooldridge, L.J., Worden, R.H., Griffiths, J. and Utley, J.E.P. 2017. Clay-coated sand grains in petroleum reservoirs: understanding their distribution via a modern analogue. *Journal of Sedimentary Research*, **87**, 338–352, https://doi.org/10.2110/jsr.2017.20

Wooldridge, L.J., Worden, R.H., Griffiths, J. and Utley, J.E.P. 2019*a*. Clay-coat diversity in marginal marine sediments. *Sedimentology*, **66**, 1118–1138, https://doi.org/10.1111/sed.12538

Wooldridge, L.J., Worden, R.H., Griffiths, J. and Utley, J.E.P. 2019*b*. How to quantify clay-coat grain coverage in modern and ancient sediments. *Journal of Sedimentary Research*, **89**, 135–146, https://doi.org/10.2110/jsr.2019.6

Worden, R.H. and Morad, S. 2000. Quartz cementation in oil field sandstones: A review of the key controversies. *International Association of Sedimentologists Special Publication*, **29**, 1–20, https://doi.org/10.1002/9781444304237.ch1

Worden, R.H. and Morad, S. 2003. Clay minerals in sandstones: controls on formation, distribution and evolution. *International Association of Sedimentologists Special Publication*, **34**, 3–41, https://doi.org/10.1002/9781444304336.ch1

Worden, R.H., Armitage, P.J. *et al.* 2018*a*. Petroleum reservoir quality prediction: overview and contrasting approaches from sandstone and carbonate communities. *Geological Society, London, Special Publications*, **435**, 1–31, https://doi.org/10.1144/sp435.21

Worden, R.H., Bukar, M. and Shell, P. 2018*b*. The effect of oil emplacement on quartz cementation in a deeply buried sandstone reservoir. *AAPG Bulletin*, **102**, 49–75, https://doi.org/10.1306/02071716001

Worden, R., Griffiths, J. *et al.* 2020. Chlorite in sandstones. *Earth-Science Reviews*, **204**, 103105, https://doi.org/10.1016/j.earscirev.2020.103105

Wu, C., Bhattacharya, J.P. and Ullah, M.S. 2015. Paleohydrology and 3D facies architecture of ancient point bars, Ferron Sandstone, Notom Delta, south-central Utah, USA. *Journal of Sedimentary Research*, **85**, 399–418, https://doi.org/10.2110/jsr.2015.29

Wu, C., Ullah, M.S., Lu, J. and Bhattacharya, J.P. 2016. Formation of point bars through rising and falling flood stages: Evidence from bar morphology, sediment transport and bed shear stress. *Sedimentology*, **63**, 1458–1473, https://doi.org/10.1111/sed.12269

Xi, K., Cao, Y. *et al.* 2015. Quartz cement and its origin in tight sandstone reservoirs of the Cretaceous Quantou formation in the southern Songliao basin, China. *Marine and Petroleum Geology*, **66**, 748–763, https://doi.org/10.1016/j.marpetgeo.2015.07.017

Xia, H., Perez, E.H. and Dunn, T.L. 2020. The impact of grain-coating chlorite on the effective porosity of sandstones. *Marine and Petroleum Geology*, **115**, 104237, https://doi.org/10.1016/j.marpetgeo.2020.104237